Reconstruction of Concentration-Dependent Material Properties in Electrochemical Systems

RECONSTRUCTION OF CONCENTRATION-DEPENDENT

MATERIAL PROPERTIES IN ELECTROCHEMICAL SYSTEMS

BY

ATHINTHRA KRISHNASWAMY SETHURAJAN, B.Tech.

A THESIS

SUBMITTED TO THE SCHOOL OF COMPUTATIONAL SCIENCE & ENGINEERING

AND THE SCHOOL OF GRADUATE STUDIES

OF MCMASTER UNIVERSITY

IN PARTIAL FULFILMENT OF THE REQUIREMENTS

FOR THE DEGREE OF

MASTER OF SCIENCE

Master of Science (2014)   McMaster University

(Computational Science & Engineering)   Hamilton, Ontario, Canada

TITLE: Reconstruction of Concentration-Dependent Material Properties in Electrochemical Systems

AUTHOR: Athinthra Krishnaswamy Sethurajan

                           B.Tech., (Chemical Engineering)

                           Anna University, Chennai, India

SUPERVISOR: Dr. Bartosz Protas

NUMBER OF PAGES: xiii, 70

To my Amma and Appa

Abstract

In this study we develop a computational approach to the solution of an inverse modelling problem concerning the material properties of electrolytes used in Lithium-ion batteries. The dependence of the diffusion coefficient and the transference number on the concentration of Lithium ions is reconstructed based on the concentration data obtained from an in-situ NMR imaging experiment. This experiment is modelled by a 1D time-dependent PDE describing the evolution of the concentration of Lithium ions with prescribed initial concentration and fluxes at the boundary. The material properties that appear in this model are reconstructed by solving a variational optimization problem in which the least-square error between the experimental and simulated concentration values is minimized. This optimization problem is solved using an innovative gradient-based method in which the gradients are obtained with adjoint analysis. In the thesis we develop and validate a computational framework for this reconstruction problem. Reconstructed material properties are presented for a lab-manufactured and a commercial battery electrolyte providing insights which complement available experimental results.

Acknowledgements

I owe my very sincere thanks to my supervisor Dr. Bartosz Protas for his patience and infinite support. His encouragement and close guidance helped me tremendously in my research work and completion of this thesis. With great excitement I am looking forward to do my PhD studies under his supervision.

I would like to thank Dr. Sergey Krachkovskiy and Dr. Gillian Goward for providing the experimental data necessary for this research work. Countless discussions with them have given me a great insight about various aspects this research and helped me in understanding the experimental setup and the electrochemical process. I would also like to thank Dr. Vladislav Bukshtynov for his code, which served as the starting point for this research work.

It was an absolute delight to work closely with Dr. Adam Gully, Dr. Seshasai Srinivasan and Dr. Jamie Foster in a research team. They have been very courteous and encouraging during our discussions. They were also instrumental in building a friendly and fun-filled atmosphere in the group.

I would also like to thank all staff, faculty members and students of School of Computational Science and Engineering and Department of Mathematics for their warm support and making my stay pleasant.

I am thankful to Dr. Ion Halalay and Dr. Giles Richardson and members of APC-LIB

Symbols

D^+ Diffusion coefficient of positive ion

D^- Diffusion coefficient of negative ion

t_+ Transference number of positive ion

$\mathcal{J}$ Cost

τ Step length in gradient direction

$\tilde{c}$ In-situ experimental concentration

A Cross-sectional area of the cell

c Salt concentration

c^* Solution of adjoint system obtained by perturbing D

c^{**} Solution of adjoint system obtained by perturbing t_+

c_i Initial concentration

c_o Solvent concentration

c_{Li+} Concentration of Lithium ion

c_s Salt concentration

c_{TFSI^-} Concentration of $TFSI^-$ ion.

D Diffusion coefficient

D' Perturbation direction for D

D_f Fick's diffusion coefficient

D_m Maxwell-Stefan's diffusion coefficient

F Faraday's constant

i Applied current

j_{cur}^- Flux of negative ions due to current

j_{diff}^- Flux of negative ions due to diffusion

j_{net}^- Total flux of negative ions

L Length of the cell

T Final time value

t_+' Perturbation direction for t_+

V_m^o Molar volume of solvent

V_m^s Molar volume of salt

Contents

List of Figures

Chapter 1

Introduction

Lithium (Li) ion batteries are popular electrochemical power storage devices and are used in a wide range of electronic devices around the world. Significant research efforts are being invested into Li-ion batteries right now, because of their potential applications in next generation automotives [21] and green technology [5]. A complete understanding of the physics and electro-chemistry behind the working of Li-ion batteries is necessary to further improve their efficiency and performance.

Many researchers across the world have tried to come up with mathematical models for Li-ion batteries for analyzing and optimizing their performance. Two main types of models that are widely used are equivalent circuit models [4] and physics-based models [24]. Both types of models have their own advantages and disadvantages, but to understand the complex behavior of the batteries at various scales [27], physics based models are preferred.

In physics-based models, different physical components are modeled separately and put together as a closed system of equations in which the individual components are allowed to interact with each other. A typical Li-ion battery is made up of solid and

liquid components. Solid components constitute the anode and the cathode which stores energy in the form of lithium atoms and also helps conduct negatively charged electrons to the external circuit. The liquid component of the battery is an electrolyte that is made up of a Li-based salt and a suitable solvent. The electrolyte helps to shunt positively charged Lithium ions across the electrodes and hence completes the circuit. The interaction of solid and liquid components takes place at the solid-liquid interface inside the battery.

Transport of lithium as atoms in the electrode and as ions in the electrolyte is assumed to be a diffusion-based process in most of the physics-based models [1, 7]. The transport of lithium in the electrolyte is of particular interest in this study. Lithium is transported as positively charged ions and they are influenced by the existing electric potential inside the battery. The main material properties that are involved in the transport of Li ions in the electrolyte are the electrical conductivity, the diffusion coefficient and the transference number. Knowledge about these properties of different electrolytes not only helps us to use them in the transport model, but also tells us about the intrinsic nature of the material under consideration. Diffusion coefficient and transference number are the properties in the focus of this study, as their measurement methods are difficult and not well developed.

Diffusion coefficient is typically measured as a constant number using Stokes-Einstein's relation [9], NMR spectroscopy [22] and by inverse calculations using potentiostatic and galvanostatic measurements [28]. The transference number of Li ion, which is defined as the fraction of applied current carried by the Li ion in the electrolyte, is another important material property. In low concentration ranges it is approximated

as the ratio of diffusion coefficients as shown below [11]

$$t_+ = \frac{D^+}{D^+ + D^-}.$$

(1.1)

Inverse calculations using galvanostatic and potentiostatic experiments are also used to estimate the transference number in electrolytic solutions [12]. In all the above mentioned methods, the diffusion coefficient and the transference number are measured as constant numbers. On the other hand, there are various studies which indicate that the diffusion coefficient and the transference number are not constant and they vary with state variables such as the concentration [15]. This fact has been confirmed by repeating the above mentioned measurements on electrolytes of various concentrations [26]. In addition, modeling studies also provide evidence that models with concentration-dependent material properties more accurately predict the behavior of battery systems [16]. Motivated by these evidence, this study attempts to develop and validate a tool that estimates concentration-dependent diffusion coefficient and transference number of the electrolyte by solving an inverse problem using experimental data.

An Inverse problem is a framework that converts observed measurements into information about the system or the object. For example, a galvanostatic experiment measures the variation in potential with time for a constant current applied through the electrolyte. With this measurement, an inverse calculation can estimate the material properties of the electrolyte such as diffusion coefficient, transference number and conductivity. Inverse problems are also an area of study that receives significant attention in many research fields such as medicine [18], earth sciences [8], image processing [2], astronomical sciences [19] etc.. Specifically, inverse problems in which one

estimates material properties as a function of space are well researched and understood and they serve as an important tool in modern non-invasive techniques [6] in medical and geological applications. In most of these applications inverse problem is posed as an optimization problem constrained by Partial Differential Equations (PDE). Use of adjoint analysis [23] to solve optimization problems constrained by PDE, for finding control parameters dependent on space, time and state, is also well understood and effectively used in advanced optimization algorithms.

Inverse problems also finds their application in estimating material properties of Li-ion battery electrolyte. A research study by M. Klett et al. [13] uses concentration data collected using NMR imaging technique to estimate the diffusion coefficient and transference number as constants. That study uses COMSOL software package to solve the PDE models and MATLAB optimization algorithm. That study is taken as a primary reference for our experimental setup and data collection. The novelty of our research study is that we propose a method to estimate material properties as a function of concentration with the same experimental effort that has been outlined by M. Klett et al.

Solving an inverse problem to estimate the state dependent material properties has been documented for a purely diffusive multi-dimensional model by V. Bukshtynov et al. [3]. In that study, solution to the inverse problem is obtained by solving an optimization problem using adjoint analysis and the diffusion coefficient is estimated for a manufactured data. It also addresses the various computational challenges related to accurate and efficient evaluation of cost functional gradients for optimization. Taking it as a primary reference for the computational setup, the current study was carried out to estimate two material properties (diffusion coefficient and transference

number) that appear in the model for Li transport in electrolyte, as a function of concentration. Although the reference study uses a model simpler than the one used here, the general guidelines that it provides are very relevant for our research study. The plan of this thesis is as follows: The experiment and the mathematical model that is suitable for the problem are first outlined in chapter 2, then the problem of estimating material properties is defined and the methodology for estimating them is outlined in chapter 3. Then in the chapter 4, various approaches to validate the method and the algorithm are outlined and the results of validation is presented. In chapter 5, the estimated material properties for real battery electrolytes that are prepared in lab and that are commercially available are presented and compared against the material properties measured by other methods and conclusions are drawn in chapter 6.

Chapter 2

Material Transport in Electrochemical System

2.1   Experimental Setup

Li-ion battery electrolyte is typically made by dissolving a Lithium-based salt in an organic solvent. Lab-manufactured electrolyte used in our study is Lithium bis(trifluoro-methanesulfonyl)imide (LiTFSI) dissolved in propylene carbonate. When dissolved in a solvent, LiTFSI will decompose into its ionic forms Li^+ and $TFSI^-$. If a differential electric potential is applied to this electrolyte, these ions migrate causing electric current to flow through the electrolyte. This ion migration charecterizes the material properties associated with electrolytes. As our goal is to reverse estimate the material properties from the material transport, a simple experiment was setup by our collaborator Dr. Sergey Krachkovisky under the supervision of Dr. Gillian Goward from the Department of Chemistry, McMaster University. With his expertise in NMR imaging [15] our collaborator has designed and developed the experimental
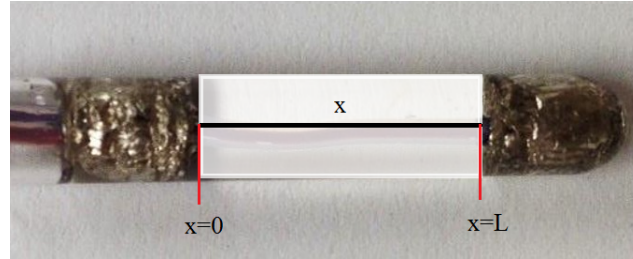
Figure 2.1: Schematic diagram of experimental setup featuring Lithium Electrodes.

tools and method described in this section.

The experimental setup shown in fig. 2.1 is a cylindrical cell whose length is characterized by spatial dimension x. The cell is filled with electrolyte of 1000 mol/m^3 salt concentration and sealed with Lithium electrodes. An In-Situ NMR (Nuclear Magnetic Resonance) imaging technique [22] was used to estimate the concentration of ions present in the electrolyte when the current was passed through the cell. This experiment is hereafter referred to as an "in-situ experiment". In this experiment a NMR probe was allowed to scan through the region of cell filled with electrolyte and measure the intensity of electromagnetic radiation emitted by Fluorine atoms present in the $TFSI^-$ ion due to the presence of a magnetic field. As it is assumed that the concentration of ions is directly proportional to the intensity of electromagnetic wave emitted by them, the intensity measurement is a indirect measure of the concentration of $TFSI^-$ ions present in the electrolyte. As NMR probe scans through the length of the cell, it measures the intensity of emitted electromagnetic wave across the cell and gives us the intensity profile of the entire cell as output.

Reference data was collected at the beginning of the experiment when no current flowing, as the concentration of the salt in the electrolyte was homogeneous throughout the cell. Then, a constant current was allowed to flow through the cell and the intensity profile was collected at equal time intervals. The intensity measurements

Figure 2.2: Intensity distribution across the cell - Different shades of color denotes measurement at different time levels

obtained by our collaborators are shown in fig. 2.2.

The measurement denoted as '0 hours' in fig.2.2 will serve as the reference corresponding to the homogeneous 1000 mol/m^3 concentration. With this measurement and the assumption that the intensity is proportional to the concentration, the concentration distribution at all other time levels can be obtained. fig. 2.3 shows the corresponding concentration profiles obtained from electromagnetic wave intensity measurements at various time levels. In this figure we can see that the concentration values become

polarized as time progresses, which is what we would expect to happen when negative ions move towards the positively charged electrode.

Similarly, this experiment was also performed with a commercial electrolyte manufactured by from Novalyte Ltd.. The commercial electrolyte is made up of $LiPF_6$ dissolved in 1:1 volume mixture of Ethylene Carbonate (EC) and DiMethyl Carbonate (DMC). Since both $LiPF_6$ and $LITFSI$ molecules yields one positive ion (Li^+) and one negative ion ($TFSI^-$ or PF_6^-), the material transport model applicable to both electrolytes will be same.

To compare the estimated diffusion coefficient, another set of experiments was carried out andwill be referred to as "ex-situ experiment". NMR self-diffusion technique is used here to measure the diffusion coefficient of both positive and negative ions in the electrolyte. This experiment was carried out repeatedly for electrolytes of different concentrations to obtain a map of diffusion coefficient as a function of concentration. For further information about NMR self diffusion experiment, the readers are recommended to read the cited article by William S. Price [22].

2.2   Mathematical Modeling

The following assumptions are made for modeling the ion transport in electrolyte.

Assumptions 1

   i. Isothermal conditions.

   ii. Salt is assumed completely ionized i.e., no neutral ion pairs or clusters exists in the solution.

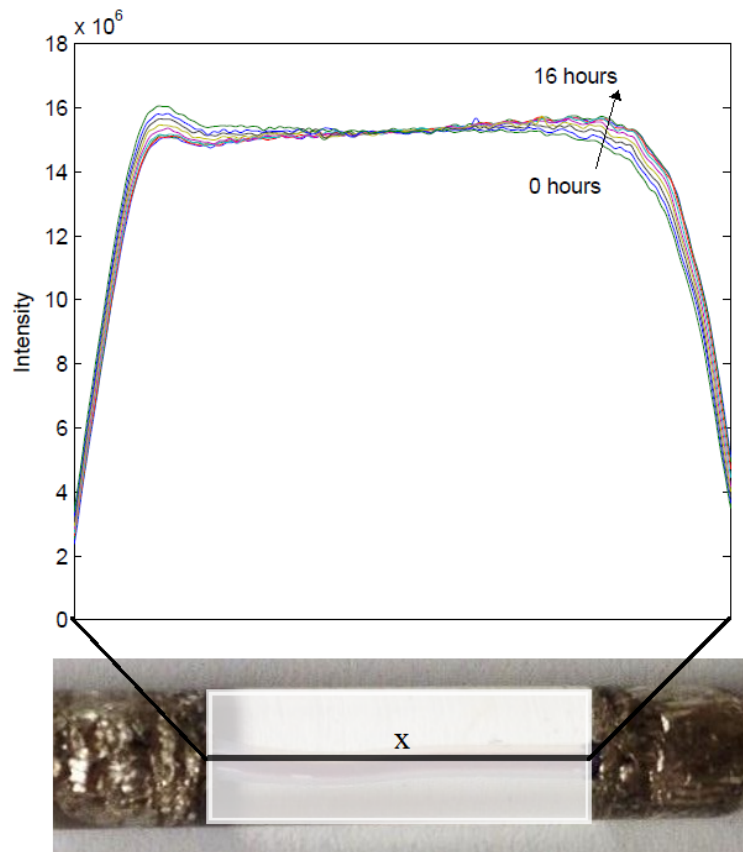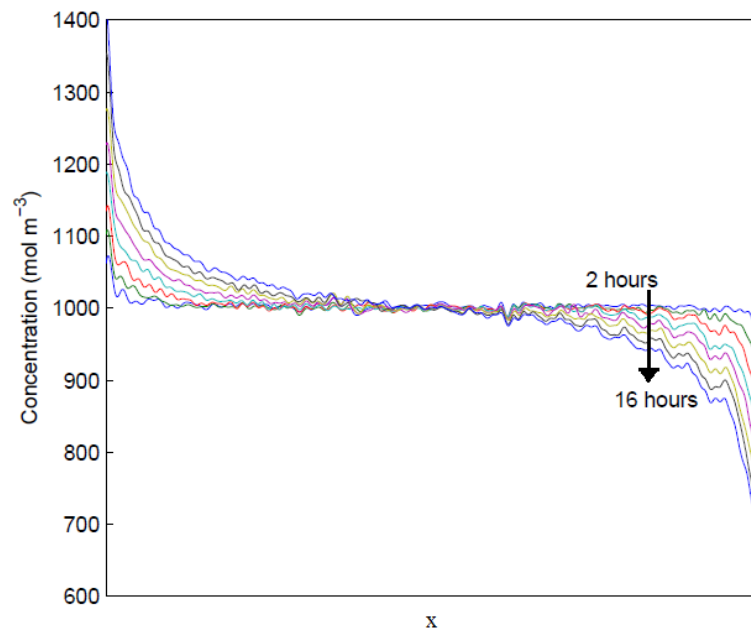Figure 2.3: Concentration distribution across the cell - Different shades of color denotes measurement at different time levels

iii. *Ion transport occurs only through the length of the cell and any transport in the radial direction of the cell is neglected. the Domain of the model is [0,L] $\subset \mathbb{R}$, where L is the length of the electrolyte region in cell as shown in fig. 2.1*

iv. *The system is electrically neutral, which implies $c_{Li^+} = c_{TFSI^-} = c_s$.*

v. *Advection other than due to the electric potential is assumed negligible.*

In this study two types of models are considered, namely, Maxwell-Sefan's model and Fick's model. These two models differ only in their approach to model diffusion. Maxwell-Stefan's theory assumes that the diffusion is driven by gradient of the chemical potential. On the other hand, Fick's theory postulates that the diffusion is driven by gradient of the concentration. Though these two models differ in how the diffusion process is represented, the transport PDE corresponding to these models are very similar to one another.

2.2.1   Maxwell-Stefan's Model

Because of assumption (v), transport of ions is influenced only by two phenomena, namely, the diffusion and the migration due to applied potential. Both these phenomena can be modeled separately. Since experimental data shows the concentration distribution of anion ($TFSI^-$ or PF_6^-), the material transport based on negative migration will be derived.

The flux of anions due to diffusion (denoted j_{diff}^-) occurs due to the combined effect of diffusion of ions and solvent in opposite directions because of differing chemical potentials. If D_m is assumed to be the Maxwell-Stefan diffusion coefficient, the diffusion

flux of cation can be written as eqn. (2.1) [20] valid on $x \in [0, L]$

$$j_{diff}^- = -\left(1 + \frac{c_s}{c_o}\right) D_m \frac{\partial c_s}{\partial x}. \tag{2.1}$$

In eqn. (2.1), c_o is the concentration of the solvent given by expression $c_o = (1 - V_m^s)/V_m^o$. Since the total concentration in the system is $c_{tot} = c_o + c_s$, the expression $1 + \frac{c_s}{c_o}$ can also be represented as $\frac{c_{tot}}{c_o}$.

The flux of anions due to applied current is the product of the fraction of the current carried by anion and the total flux due to the current and is given in eqn.(2.2) [20].

$$j_{cur}^- = -\frac{(1 - t_+) i}{FA}, \tag{2.2}$$

where F is Faraday's constant used to convert amperes to moles. As t_+ is the transference number of cations (Li^+), $1 - t_+$ will be the fraction of the current carried by the anion.

The total (or net) flux of anions is $j_{net}^- = j_{diff}^- + j_{cur}^-$. The law of conservation for the salt dissolved in the solvent is written as [20],

$$\frac{\partial c_s}{\partial t} + \frac{\partial}{\partial x}\left[V_m^o c_o \left(j_{net}^-\right)\right] = 0, \quad x \in (0, L) \text{ and } t \in [0, T], \tag{2.3}$$

where T is the final time of the experimental data. By eliminating j_{net}^- in eqn. (2.3) and by using the relation $V_m^o c_o + V_m^s c_s = 1$, we obtain a PDE for c_s

$$\frac{\partial c_s}{\partial t} = \frac{\partial}{\partial x}\left[(1 - c_s V_m^s)\left(\frac{c_{tot}}{c_0} D_m \frac{\partial c_s}{\partial x} + \frac{(1 - t_+) i}{FA}\right)\right], \quad x \in (0, L) \text{ and } t \in [0, T]. \tag{2.4}$$

12

Eqn. (2.4) requires initial and boundary conditions for unique solution. As the boundaries are isolated, we can assume that the net flux (j_{net}^-) is zero there. By substituting the expression of fluxes from eqn. (2.1) and (2.2) in this condition, we can derive the following the boundary condition.

$$\left.\frac{\partial c}{\partial x}\right|_{x=0,L} = -\frac{(1-t_+)\,i}{\frac{c_{tot}}{c_0}D_m F A} \tag{2.5}$$

To simplify the notations, the concentration variable c_s will be hereafter represented as c.

Since the concentration was homogeneous in the cell at the beginning of the experiment, it is assumed that initial concentration is constant (c_i) and equal to 1000 mol/m^3

$$c|_{t=0} = c_i. \tag{2.6}$$

To simplify the system equation in Maxwell-Stefan's model, we denote

$$D = (1 - cV_m^s)\frac{c_{tot}}{c_0}D_m. \tag{2.7}$$

Using equation (2.7), we can then transform between the variables D and D_m. The governing system of Maxwell-Stefan's model can now be consolidated as

$$\frac{\partial c}{\partial t} = \frac{\partial}{\partial x}\left[D\frac{\partial c_s}{\partial x} + (1 - c_s V_m^s)\frac{(1-t_+)\,i}{FA}\right], \tag{2.8a}$$

$$\left.\frac{\partial c}{\partial x}\right|_{x=0,L} = -\frac{(1-t_+)\,i}{DFA}\left(1 - c_s V_m^s\right), \tag{2.8b}$$

$$c|_{t=0} = c_i. \tag{2.8c}$$

13

There are four material properties that are involved in the model equation $(V_m^s, V_m^o, D_s$ and $t_+)$, out of which two are molar volumes of the salt and solvent (V_m^s and V_m^o, respectively). The molar volumes are intrinsic properties and are measured with simple experimental techniques. These values of the molar fluxes are also experimentally measured by our collaborators.

2.2.2 Fick's Model

To eliminate uncertainties in the measurement of the molar volumes, we can use an alternative model which is derived from Fick's law. In this formulation j_{cur}^- is the same as the expression in eqn. (2.2), but the expression for diffusion flux and law of conservation is different and given as

$$j_{diff}^- = -D_f \frac{\partial c}{\partial x}, \tag{2.9}$$

$$\frac{\partial c}{\partial t} + \frac{\partial j_{net}^-}{\partial x} = 0, \tag{2.10}$$

where D_f is Fick's diffusion coefficient. Using these expression our governing system can be rewritten as

$$\frac{\partial c}{\partial t} = \frac{\partial}{\partial x}\left[D_f \frac{\partial c}{\partial x} + \frac{(1 - t_+)\,i}{FA} \right] \tag{2.11a}$$

$$\frac{\partial c}{\partial x}\bigg|_{x=0,L} = -\frac{(1 - t_+)\,i}{D_f FA} \tag{2.11b}$$

$$c|_{t=0} = c_i \tag{2.11c}$$

For Fick's model D_f is same as D defined in eqn. (2.7).

The diffusion coefficients of both Maxwell-Stefan's model and Fick's model are different and they will have different values in the same experiment. Fick's diffusion coefficient is popular across the modeling research community and available as a constant for popular electrolytes in the literature. On the other hand, Maxwell-Stefan's diffusion coefficient is not as popular but Maxwell-Stefan's theory is more comprehensive and does not exclude the possibility of negative diffusion coefficient [14].

The following parts of this thesis will explore the ways to estimate the diffusion coefficient and the transference number as a function of the concentration based on the available experimental data.

Chapter 3

Inverse Problem for Reconstruction of Transport Coefficients

3.1 Reconstruction as Optimization Problem

A common approach to reconstruct material properties is to use some strategy to minimize the least-square error between the experimental and simulated concentration values. Thus, an optimization problem is posed where the least-square error is the cost functional that has to be minimized with respect to the material properties, namely, the diffusion coefficient and the transference number, as the control parameters.

$$\mathcal{J}(D, t_+) = \frac{1}{2} \int_0^T \int_0^L \left(c(x, t; D, t_+) - \tilde{c}(x, t) \right)^2 \, dx dt, \tag{3.1}$$

where the dependence of concentration $c(.; D, t_+)$ is given by the mathematical model described in eqn. (2.8) and (2.11). The minimization problem is posed as

$$\min_{D, t_+} \mathcal{J}. \tag{3.2}$$

This optimization problem can be stated in two distinct ways

$$\textbf{P1}: \qquad\qquad [\hat{D}, \hat{t}_+] = \underset{[t_+, D] \in \mathbb{R}^2}{\operatorname{argmin}} \mathcal{J} \qquad \text{and}$$

$$\textbf{P2}: \qquad\qquad [D(c), t_+(c)] = \underset{[t_+, D] \in \mathcal{U}}{\operatorname{argmin}} \mathcal{J},$$

where $\mathcal{U}$ is the function space with a Hilbert structure. The problem posed in P1 is simple, as the solution is obtained as a constant vector in real space $\mathbb{R}^2$. This type of inverse problem is rather straight forward and solution methodologyia already documented [13]. On the other hand, problem P2 is not trivial as one seeks there to identify $D(c)$ and $t_+(c)$ as a function of concentration c, and a major part of this thesis is devoted to the development of a solution strategy for P2.

The problem P2 is an unconstrained optimization problem and hence the first order optimality condition requires that the gradient of cost functional $\mathcal{J}$ with respect to control parameters to vanish. The symbols $\nabla_D \mathcal{J}$ and $\nabla_{t_+} \mathcal{J}$ will denote gradients of cost functional with respect to D and t_+, respectively. With the help of these gradients, local minima for D and t_+ can be obtained using a simple-gradient decent algorithm.

$$
\begin{cases}
D^{(n+1)} = D^{(n)} - \tau_D^{(n)} \nabla_D \mathcal{J}(D^{(n)}, t_+^{(n)}) & n = 1, 2, ..., \\
t_+^{(n+1)} = t_+^{(n)} - \tau_{t_+}^{(n)} \nabla_{t_+} \mathcal{J}(D^{(n+1)}, t_+^{(n)}) & n = 1, 2, ...,
\end{cases}
\tag{3.3}
$$

where τ_D^n and $\tau_{t_+}^n$ are the length of the decent step at iteration n and $D^{(1)}$ and $t_+^{(1)}$ are the initial guesses. Local minima of D and t_+ can therefore be computed as $\widehat{D} = \lim_{n \to \infty} D^n$ and $\widehat{t}_+ = \lim_{n \to \infty} t_+^n$, respectively.

There are many ways of formulating a gradient descent algorithm for problem P2 and eqn. (3.3) is just one possibility. In this method the values for D and t_+ are updated one after the other in the spirit of Gauss-Seidel iteration for solving linear systems.

In our study, optimal solutions of problem P1 is assumed to be the initial guess of problem for reducing the computational time and to avoid local optima in higher cost regions and it can be expressed as following

$$
[D(c)^{(1)}, t_+(c)^{(1)}] = [\hat{D}, \hat{t}_+].
\tag{3.4}
$$

3.2   Gradient of Cost Functional

Gradient of the cost functional in a function space is the key ingredient for solving problem P2. Gradients can be derived using adjoint analysis with the directional derivative of cost functional. A similar derivation for a simple diffusion system is done by Bukshtynov et al.[3]. Following the same technique, the derivation of gradient of cost functional $(\nabla_D \mathcal{J})$ with respect to diffusion coefficient (D) is shown below.

To obtain the gradient of $\mathcal{J}$ with respect to D, we first have to define the directional

derivative (Gâteaux) of $\mathcal{J}$ with respect to D.

$$\mathcal{J}'(D, t_+; D') = \lim_{\epsilon \to 0} \epsilon^{-1} \left(\mathcal{J}(D + \epsilon D', t_+) - \mathcal{J}(D, t_+) \right), \tag{3.5}$$

where D' is the perturbation of the control variable D. To calculate the gradient of $\mathcal{J}$, Riesz representation of directional derivative is used [3].

$$\mathcal{J}'(D, t_+; D') = \langle \nabla_D \mathcal{J}, D' \rangle_{\mathcal{X}}, \tag{3.6}$$

where $\langle ., . \rangle$ is the inner product in the functional (Hilbert) space $\mathcal{X}$. The directional derivative of $\mathcal{J}$ in the form represented in eqn. (3.1) is computed as

$$\mathcal{J}'(D, t_+; D') = \int_0^T \int_0^L \left[c(x, t; D, t_+) - \tilde{c}(x, t) \right] c'(x, t; D, D') dx dt, \tag{3.7}$$

where c' is the solution of PDE system obtained after perturbing the PDE system ((2.8) or (2.11)).

3.2.1 Maxwell-Stefan's Model

As the perturbation system depends on the specific version of the governing equation, we have to deal with them separately. Maxwell-Stefan's model is considered first and the following transformations are invoked to begin the derivation of the cost functional gradient

$$V(x, t) = \int_{c_\alpha}^{c(x,t)} D(s) ds \quad \text{on domain x} \in [0,L] \text{ and t} \in [0,T], \tag{3.8}$$

19

where $[c_\alpha, c_\beta]$ is the identifiability interval $\mathcal{I}$ defined as the range of concentration values spanned by the solution of PDE system (2.4)-(2.6). Then we denote

$$Q(x,t) = (1 - c(x,t)V_m^s)\frac{(1-t_+)i}{FA}. \tag{3.9}$$

Using these two simplifications, the perturbation system for governing system (2.4)-(2.6) can be rewritten as

$$\frac{\partial c'}{\partial t} = \frac{\partial}{\partial x}\left(\frac{\partial V'}{\partial x} + Q'\right) \qquad \text{x} \in \text{(0,L) t} \in \text{(0,T]}, \tag{3.10a}$$

$$\left.\left(\frac{\partial V'}{\partial x} + Q'\right)\right|_{x=0,L} = 0 \qquad\qquad\qquad \text{t} \in \text{[0,T]}, \tag{3.10b}$$

$$c'|_{t=0} = 0 \qquad\qquad\qquad \text{x} \in \text{[0,L]}. \tag{3.10c}$$

Multiplying eqn. (3.10a) by adjoint variable $c*$ and integrating over time and space, we get

$$\int_0^L \int_0^T \frac{\partial c'}{\partial t}c^* dtdx = \int_0^T \int_0^L \left[\frac{\partial^2 V'}{\partial x^2}c^* + \frac{\partial Q'}{\partial x}c^*\right] dxdt. \tag{3.11}$$

By re-organizing eqn. (3.11) and integrating it by parts we get

$$\int_0^L \left[[c'c^*]_0^T - \int_0^T \frac{\partial c^*}{\partial t}c' dt\right] dx$$
$$= \int_0^T \left[\left[\frac{\partial V'}{\partial x}c^*\right]_0^L - \int_0^L \frac{\partial V'}{\partial x}\frac{\partial c^*}{\partial x}dx + [Q'c^*]_0^L - \int_0^L Q'\frac{\partial c^*}{\partial x}dx\right] dt. \tag{3.12}$$

Using eqn. (3.10b) and (3.10c), we can eliminate a number of boundary terms and then integrate the term with $\frac{\partial V'}{\partial x}$ by parts one more time we get

$$
\int_0^L \left[[c'c^*]_{t=T} - \int_0^T \frac{\partial c^*}{\partial t} c' dt \right] dx
$$
$$
= \int_0^T \left[-\left[\frac{\partial c^*}{\partial x} V' \right]_0^L + \int_0^L V' \frac{\partial^2 c^*}{\partial x^2} dx - \int_0^L Q' \frac{\partial c^*}{\partial x} dx \right] dt. \quad (3.13)
$$

Perturbation variables V' and Q' can be then expressed as

$$
V'(x,t) = \int_{c_\alpha}^{c(x,t)} D'(s) ds + D(c) c'(x,t; D'), \quad (3.14)
$$
$$
Q'(x,t) = -\left((1 - c(x,t) V_m^s) \frac{dt_+}{dc} c'(x,t; D') + V_m^s c'(x,t; D')(1 - t_+) \right) \frac{i}{FA}. \quad (3.15)
$$

We can assume adjoint system (in the same domain as PDE system (2.8)) in the form

$$
-\frac{\partial c^*}{\partial t} = D \frac{\partial^2 c^*}{\partial x^2} + \left((1 - c V_m^s) \frac{dt_+}{dc} + V_m^s (1 - t_+) \right) \frac{i}{FA} \frac{\partial c^*}{\partial x} + (c - \tilde{c}), \quad (3.16a)
$$
$$
\left. \frac{\partial c^*}{\partial x} \right|_{x=0,L} = 0, \quad (3.16b)
$$
$$
\left. c^* \right|_{t=T} = 0. \quad (3.16c)
$$

With this assumed form of adjoint system, we can eliminate most of the terms from eqn. (3.13) and are left with expression for the directional derivative of cost functional

$$
\mathcal{J}'(s) = \int_0^T \int_0^L \left[\int_{c_\alpha}^{c(x,t)} D'(s) ds \right] \frac{\partial^2 c^*}{\partial x^2} dx dt. \quad (3.17)
$$

The adjoint (3.16) does not have an initial condition but has a terminal condition. This terminal value problem can be solved by solving the system backward in time. With Riesz representation expressed in eqn. (3.20) we can now obtain the gradient of cost functional, which takes the following form in L_2 functional space.

$$\nabla_D^{L_2} \mathcal{J}(s) = \int_0^T \int_0^L \chi_{[c_\alpha, c(x,t)]}(s) \frac{\partial^2 c^*}{\partial x^2} dx dt, \tag{3.18}$$

where $\chi_{[a,b]} = \begin{cases} 1, & s \in [a,b] \\ 0, & s \notin [a,b] \end{cases}$.

Similarly, the directional derivative of cost functional with respect to the transference number t_+ can also be defined and from its respective Riesz representation, we can obtain the gradient of cost functional with respect to transference number

$$\mathcal{J}'(D, t_+; t_+') = \lim_{\epsilon \to 0} \epsilon^{-1} \left(\mathcal{J}(D, t_+ + \epsilon t_+') - \mathcal{J}(D, t_+) \right), \tag{3.19}$$

$$\mathcal{J}'(D, t_+; t_+') = \left\langle \nabla_{t_+} \mathcal{J}, t_+' \right\rangle_\chi, \tag{3.20}$$

where t_+' is the perturbation of the control variable t_+. We can simplify the derivation by introducing variables V and Q as defined in eqn. (3.8) and (3.9). The perturbation system will look exactly the same as the one defined for $\nabla_D \mathcal{J}$, which is given in eqn. (3.10a)-(3.10c). As a next step, we integrate perturbation equation over space and time and multiply both sides with adjoint variable c^{**}. Then we apply integration by parts and use boundary and initial conditions to eliminate boundary terms. The

resulting equation has an exact form as eqn. (3.13) but with adjoint variable c^{**}

$$\int_0^L \left[[c'c^{**}]_{t=T} - \int_0^T \frac{\partial c^{**}}{\partial t} c' dt \right] dx$$
$$= \int_0^T \left[-\left[\frac{\partial c^{**}}{\partial x} V' \right]_0^L + \int_0^L V' \frac{\partial^2 c^{**}}{\partial x^2} dx - \int_0^L Q' \frac{\partial c^{**}}{\partial x} dx \right] dt. \quad (3.21)$$

The perturbation variable V' and Q' can be expressed as following for the directional perturbation t'_+

$$V'(x,t) = D(c)c'(x,t;t'_+), \quad (3.22)$$

$$Q'(x,t) = -\left[(1 - c(x,t)V_m^s) \frac{dt_+}{dc} c'(x,t;t'_+) \right] \frac{i}{FA}$$
$$+ \left[(1 - c(x,t)V_m^s) t'_+ + V_m^s c'(x,t;t'_+)(1 - t_+) \right] \frac{i}{FA}. \quad (3.23)$$

Using V' and Q' we can finally obtain the adjoint system as

$$-\frac{\partial c^{**}}{\partial t} = D \frac{\partial^2 c^{**}}{\partial x^2} + \left((1 - cV_m^s) \frac{dt_+}{dc} + V_m^s(1 - t_+) \right) \frac{i}{FA} \frac{\partial c^{**}}{\partial x} + (c - \tilde{c}), \quad (3.24a)$$

$$\left. \frac{\partial c^{**}}{\partial x} \right|_{x=0,L} = 0, \quad (3.24b)$$

$$c^{**}|_{t=T} = 0. \quad (3.24c)$$

With this assumed form of adjoint system, we can express directional derivative of cost functional $(\mathcal{J}')$ with respect to t_+ as follows

$$\mathcal{J}' = \int_0^T \int_0^L \frac{\partial c^{**}}{\partial x} \left[1 - c(x,t)V_m^s \right] t'_+ dx dt. \quad (3.25)$$

Using Riesz representation, the gradient of cost functional in L_2 space can be expressed as

$$\nabla^{L_2}_{t_+} \mathcal{J}(s) = \int_0^T \int_0^L \frac{\partial c^{**}}{\partial x} \left[1 - c(x,t)V_m^s\right] \delta(s - c(x,t)) dx dt. \tag{3.26}$$

Eqn. (3.18) and (3.26) are the expressions of the gradient of cost functional in L_2 space for Maxwell-Stefan model. To obtain this gradient, one has to solve system and adjoint equations characterized by each control variable and obtain the gradient of cost functional in the identifiability region $\mathcal{I}$.

3.2.2 Fick's Model

For Fick's model the derivation of gradient in L_2 space is very similar and in fact the expression of the gradient of cost functional in L_2 space is exactly as eqn. (3.18) and (3.26). The difference arises only from the adjoint equation. For the control variable D the adjoint system is the following

$$-\frac{\partial c^*}{\partial t} = D\frac{\partial^2 c^*}{\partial x^2} + \frac{dt_+}{dc}\frac{i}{FA}\frac{\partial c^*}{\partial x} + (c - \tilde{c}), \tag{3.27a}$$

$$\left.\frac{\partial c^*}{\partial x}\right|_{x=0,L} = 0, \tag{3.27b}$$

$$\left.c^*\right|_{t=T} = 0, \tag{3.27c}$$

whereas for the control variable t_+ the adjoint system is

$$-\frac{\partial c^{**}}{\partial t} = D\frac{\partial^2 c^{**}}{\partial x^2} + \frac{dt_+}{dc}\frac{i}{FA}\frac{\partial c^{**}}{\partial x} + (c - \tilde{c})\,, \qquad (3.28a)$$

$$\left.\frac{\partial c^{**}}{\partial x}\right|_{x=0,L} = 0, \qquad (3.28b)$$

$$c^{**}\big|_{t=T} = 0. \qquad (3.28c)$$

Using these adjoint equation and the system mentioned in eqn. (2.11a)-(2.11c), we can find the gradient of cost functional to carry out the reconstruction of material properties that appear in Fick's model.

3.2.3   Gradient in Sobolev Space

So far we have derived gradient expression of cost functional in L_2 space , but as pointed out in [23], L_2 gradients are not suitable for the reconstruction of material properties, because they can potentially be discontinuous and undefined outside identifiability region $\mathcal{I}$. So, for the function to be smooth and continuous, we can use the gradients of cost functional in Sobolev space. By invoking Reisz representation theory again we can convert the gradients in L2 space to H1 space. For a given control variable θ we can write Riesz representation as

$$\mathcal{J}'(\theta; \theta') = \left\langle \nabla_\theta^{L_2}\mathcal{J}, \theta'\right\rangle_{L_2} = \left\langle \nabla_\theta^{H^1}\mathcal{J}, \theta'\right\rangle_{H^1}. \qquad (3.29)$$

Inner products in L_2 and H^1 spaces are defined as

$$\left\langle \nabla_\theta^{L_2} \mathcal{J}, \theta' \right\rangle_{L_2} = \int_{\mathcal{I}} \nabla_\theta^{L_2} \mathcal{J} \theta'(s) ds, \tag{3.30}$$

$$\left\langle \nabla_\theta^{H^1} \mathcal{J}, \theta' \right\rangle_{H^1} = \int_{\mathcal{I}} \left(\nabla_\theta^{H^1} \mathcal{J} \theta' + l^2 \frac{d\nabla_\theta^{H^1} \mathcal{J}}{ds} \frac{d\theta'}{ds} \right) ds, \tag{3.31}$$

where l is the Sobolev parameter. As per expression in eqn. (3.29), we equate (3.30) and (3.31) and use integration by parts to get

$$\int_{\mathcal{I}} \nabla_\theta^{L_2} \mathcal{J} \theta'(s) ds = \int_{\mathcal{I}} \left(\nabla_\theta^{H^1} \mathcal{J} \theta' - l^2 \frac{d^2 \nabla_\theta^{H^1} \mathcal{J}}{ds^2} \theta' \right) ds + \left[\frac{d\nabla_\theta^{H^1} \mathcal{J}}{ds} \theta' \right]_{c_\alpha}^{c_\beta}. \tag{3.32}$$

If we assume homogeneous Neumann boundary condition on the boundaries, we can define an ODE for conversion of gradient from L_2 space to H^1 space

$$\nabla_\theta^{L_2} \mathcal{J} = \nabla_\theta^{H^1} \mathcal{J} - l^2 \frac{d^2 \nabla_\theta^{H^1} \mathcal{J}}{ds^2} \qquad \text{on } \mathcal{I} \in (c_\alpha, c_\beta), \tag{3.33}$$

with boundary condition

$$\nabla_\theta^{H^1} \mathcal{J} \Big|_{c=c_\alpha, c_\beta} = 0. \tag{3.34}$$

This transformation is analogous to a low-pass filter that eliminates high-frequency noise and this property is necessary to eliminate the discontinuities that can arise in the L_2 gradients. The degree of noise filtration is determined by the Sobolev parameter l. Higher values of l will have smoother gradients in H^1 space. Reconstruction of all material properties, that are shown in this thesis, are done using the gradient of cost functional in Sobolev space.

Chapter 4

Computational Framework and Its Validation

4.1 Denoising Experimental data

The experimental data that has been provided, plays a key role in the reconstruction of material properties and the gradients will be very sensitive to the noise in them. So it is important to eliminate the presence of noise in the experimental data to get smooth gradients which in-turn would give us smooth reconstruction. MATLAB inbuilt filter `smooth` is used with 'sgolay' option which uses Savitzy-Golay filter, with the span of 50 points. Figure 4.1 shows the experimental data before and after denoising using MATLAB filter `smooth` and it can be clearly seen that after filtering, experimental data looks devoid of high frequency noise. This filter is applied to all experimental data used for estimating optimal constant material properties and reconstructing variable material properties.
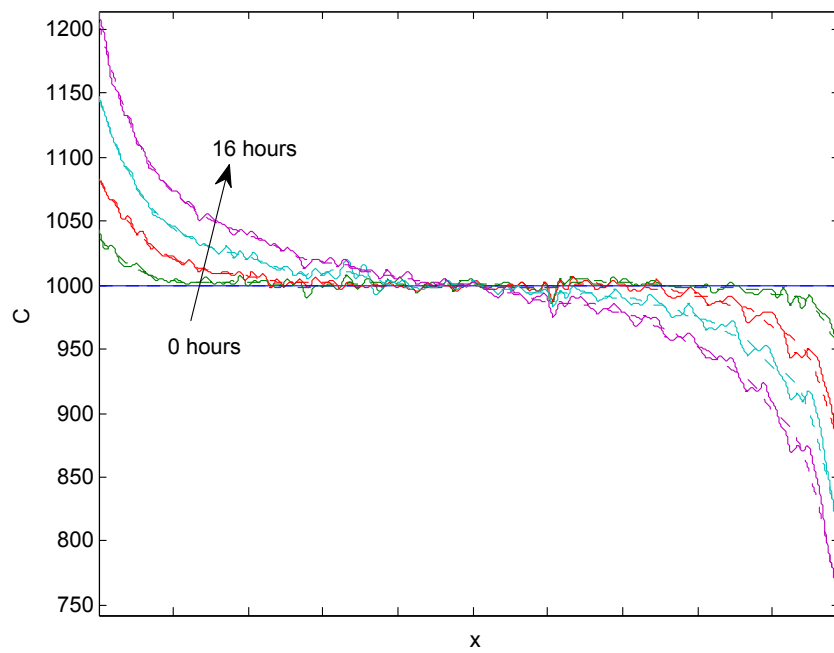
Figure 4.1: Experimental data before (solid line) and after (dashed line) denoising. Different colors indicate the experiment data at different time.

4.2   PDE Solver

All the PDEs involved in our study can be categorized as one dimensional advection-diffusion equations and have parabolic and hyperbolic components in them. They are complemented with Neumann type boundary condition in space and initial condition in time. For simplicity and reasonable accuracy, second-order accurate numerical discretization methods are used. Second-order finite difference method is used to discretize equations in space and second order Runge-Kutta time stepping scheme is used to move forward in time.

For example, let us consider PDE (2.4) with eqn. (2.7) substituted in it. Let's define an intermediate parameter H on an arbitrary time as

$$H_{j+\frac{1}{2}}^n = D(c_j^n)\frac{c_{j+1}^n - c_j^n}{\Delta x} + \left(1 - V_m^s c_j^n\right)\frac{\left(1 - t_+(c_j^n)\right)i}{FA} + O(\Delta x^2) \qquad j = 1, 3, 4.....(J),$$

$$(4.1)$$

where J+1 is the number of discrete points in the uniformly discretized space domain x, Δx is the distance between two adjacent discrete points in space so that $L = \Delta x \times J$ and j and n indicate the position in discrete space and time, respectively. Values of c in the end points of the domain, i.e., c_1 and c_{J+1} can be obtained by solving the following discretized boundary equation.

$$\frac{-3c_1^n + 4c_2^n - c_3^n}{2\Delta x^2} = -\left(1 - V_m^s c_1^n\right)\frac{\left(1 - t_+(c_1^{n-1})\right)i}{D(c_1^{n-1})FA} + O(\Delta x^2), \qquad (4.2a)$$

$$\frac{3c_{J+1}^n - 4c_J^n + c_{J-1}^n}{2\Delta x^2} = -\left(1 - V_m^s c_{J+1}^n\right)\frac{\left(1 - t_+(c_{J+1}^{n-1})\right)i}{D(c_{J+1}^{n-1})FA} + O(\Delta x^2). \qquad (4.2b)$$

Using eqn. (4.1) and (4.2) we can define time derivative of concentration as

$$\left(\frac{\partial c}{\partial t}\right)_j^n = I_j^n = \frac{H_{j+\frac{1}{2}}^n - H_{j-\frac{1}{2}}^n}{\Delta x} \qquad .j = 2, 3, 4.....(J-1) \qquad (4.3)$$

With this definition of the rate of change of concentration with time, we can step forward in uniformly discretized time domain to solve for c using second-order Runge-Kutta time stepping. In this scheme concentration at half time step is defined as

$$c_j^{n+\frac{1}{2}} = c_j^n + \frac{\Delta t I_j^{n-1}}{2}. \qquad (4.4)$$

Using $c^{n+\frac{1}{2}}$ from eqn. (4.5) we can define $I^{n+\frac{1}{2}}$ using eqn. (4.1) to (4.3)

$$c_j^{n+1} = c_j^n + \Delta t I_j^{n+\frac{1}{2}} + O(\Delta x^2) + O(\Delta t^2) \qquad \begin{cases} n = 1, 2, 3...N \\ \\ j = 2, 3...(J-1) \end{cases} , \qquad (4.5)$$

where N is the number of time steps taken to reach the final time T, ΔT is the time interval between each time step and concentration values corresponding to c^1 is given by initial condition in eqn. (2.6). For finding solution c it is necessary to perform $O(J)$ operations for each of N time steps, so we can say that computational time for solving a single PDE is $O(NJ)$. Equations of both Maxwell-Stefan's and Fick's model are solved using the described method and their respective adjoint systems are solved in similar way, but backwards in time as the adjoint system has prescribed c^* value at final time T.

The PDE solver is validated using the method of manufactured solution. In this method, a simple exponential function of space and time is assumed and the initial

condition, boundary condition and extra source term are formulated such that the assumed function satisfies the PDE system. This formulated system is then implemented in the discretized space and time and numerical solution is obtained. This numerical solution is compared against the assumed function to validate the numerical method implemented in the programming platform.

If C_n denotes numerical solution and C_r the exact solution (assumed function) of the PDE system, we can define the relative error E as follows

$$E = \frac{\|C_n - C_r\|_p}{\|C_r\|_p},$$ (4.6)

where $\|.\|_p$ is the p-norm of a vector. For the given C_r, relative error E_p is the function of Δx and Δt.

The absolute difference between the exact and numerical solution is the term $O(\Delta x^2) + O(\Delta t^2)$ in eqn. (4.5) and when we plot error vs. Δx by fixing Δt in logarithmic scale, we should expect the slope of 2. Fig. 4.2 is the logarithmic plot of relative error versus Δx. The plot confirms that the error declines with the decrease in Δx and it declines quadratically. The error saturates at the constant value for lower Δx because of of the error due to discretization in time is higher than the error due to discretization in space for sufficiently small Δx. This confirms that the PDE solver is second order accurate in space. This test also offers an insight to choose an optimal discretization length and step size in time while using this solver to solve the governing and adjoint PDEs. Fig. 4.3 the dependence of relative error on Δt. This plot, which is very similar to fig. 4.2, shows second order decay in error with respect to Δt. Both these plots demonstrates that the developed PDE solver exhibits
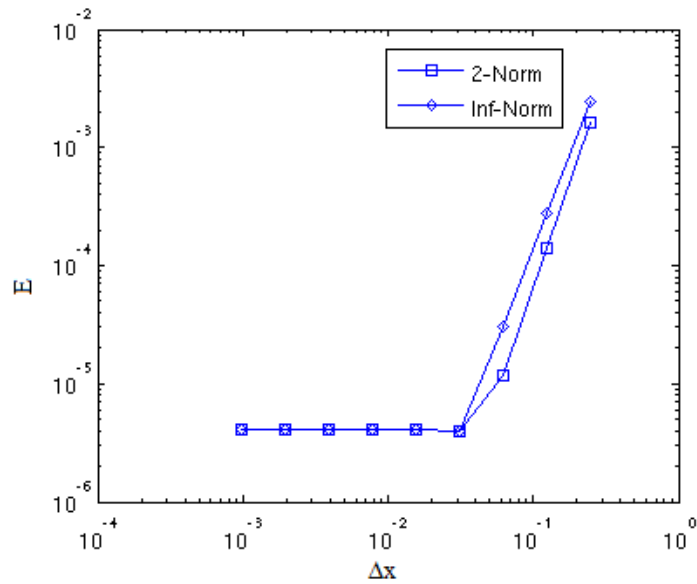
Figure 4.2: Plot of relative error E vs discretization length in space Δx. Step size in time kept constant at $\Delta t = 2.5 \times 10^{-2}$.
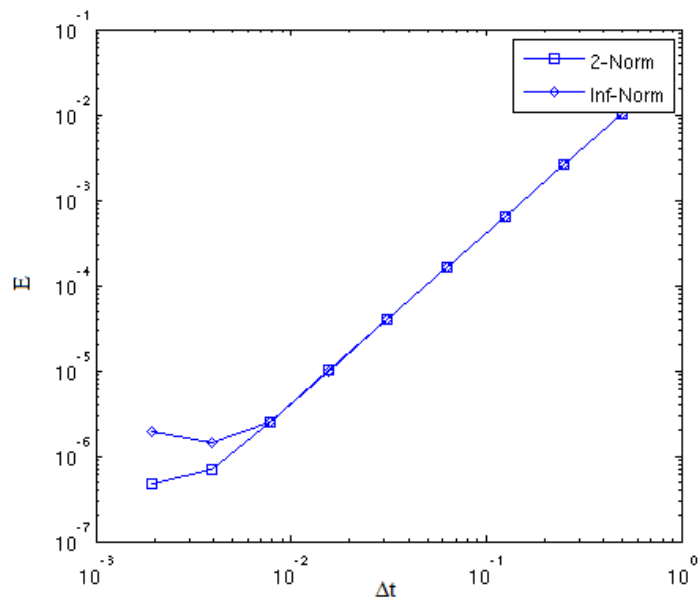

Figure 4.3: Plot of relative error E vs step size in time Δt. Discretization length in space is kept constant at $\Delta x = 2.5 \times 10^{-2}$.

expected accuracy both in space and time. This validated PDE solver used to develop the governing system and adjoint solvers necessary to reconstruct the material properties.

4.3   Solution of Optimization Problem P1

Obtaining optimal $\hat{D}$ and $\hat{t}_+$ as constants (problem P1) is the first step in the reconstruction of D(c) and $t_+(c)$ as functions of the concentration and they serve as the initial guess for the problem P2. This first step in itself can give us a insight about the material that is being used and can also be used as a credible validation of the model and experimental technique [20]. This constant parameter optimization is carried out using the inbuilt MATLAB function `fminsearch`, which uses a simplex search method. Initial guess for D is given in the order of 10^{-10} and for t_+ in the range between 0 and 1. The surface plot of the dependence of cost functional $\mathcal{J}(D, t_+)$ on D and t_+ is also generated to check the occurrence of more than one minima in the solution space.

4.4   Solution of Optimization Problem P2

Reconstructing the concentration dependent material properties is $D(c)$ and $t_+(c)$ is a task that involves various steps and they are described in following sections.

4.4.1   Gradient Validation

As we are using an optimization approach to reconstruct material properties, the gradient of cost functional with respect to material properties plays a key role in this study. So, it is very important to make sure that the gradients which are derived from adjoint analysis are accurate. To obtain the gradient of cost functional with respect to the control variable, we need to solve the system and adjoint PDEs and evaluate the expressions for gradient as mentioned for various control variables in chapter 3. To validate the gradients derived using adjoint analysis, we use a technique called "κ test". In κ test an arbitrary perturbation of control variable is assumed and the corresponding directional derivative is compared with Riesz representation that involves gradient of control variable in L_2 space. For comparison purposes, the ratio of these two parameters is defined as κ. For control variable D(c) we can define κ as

$$\kappa(\epsilon) = \frac{\epsilon^{-1}\left[\mathcal{J}(D + \epsilon D') - \mathcal{J}(D)\right]}{\int_{c_\alpha}^{c_\beta} \nabla \mathcal{J}_D^{L_2}(s)D'(s)ds}, \tag{4.7}$$

where ϵ is the perturbation size and D' is the perturbation direction. If the gradients are perfectly accurate, the parameter κ should be one, but as we use approximations while solving PDEs and while evaluating the expression for gradient, we expect κ values close to one. Fig. 4.4 is the κ-test result that validates the gradient $\nabla_D^{L_2}\mathcal{J}$. Since the validation of $\nabla_D^{L_2}\mathcal{J}$ is to make sure that the adjoint analysis is correct, κ test was carried out for a toy problem with manufactured experimental data. For κ test, three different D' functions are used (exponential, quadratic and constant) and are plotted as three distinct curves in fig. 4.4. As we expect, the κ values are close to the value one for fairly large range of ϵ and on its extreme values the accuracy drops
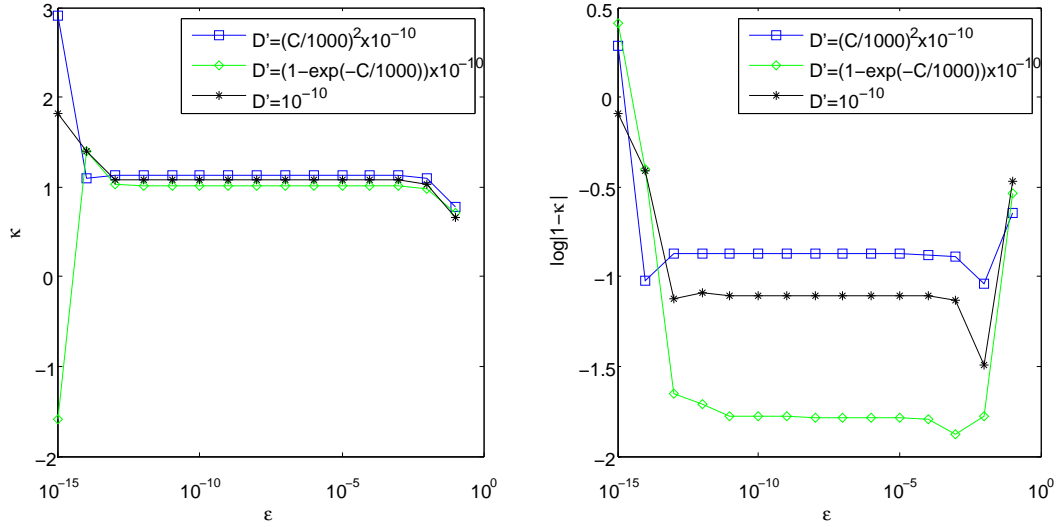
Figure 4.4: κ test to validate $\nabla_D^{L_2}\mathcal{J}$ using three different perturbation function represented in linear and log scale

rapidly. Same test for the gradient $\nabla_{t_+}^{L_2}\mathcal{J}$ is conducted and the results are presented in fig. 4.5 These tests are carried out for both the models described in chapter 2 and during various stages of code development. Satisfactory results of κ-test indicate that the cost functional gradients are sufficiently accurate to be used for the optimization algorithm

4.4.2   Reconstruction Algorithm

As discussed extensively, cost functional and its gradient play a major role in the reconstruction of material properties via the solution of problem P2 (diffusion coefficient and transference number). Reconstruction algorithm is built based on a gradient descent method using the gradients derived by solving governing and adjoint equations. Conjugate gradient method is used as an optimization method for its simplicity and its proven ability to reduce computational time. The Fletcher-Reeves conjugate
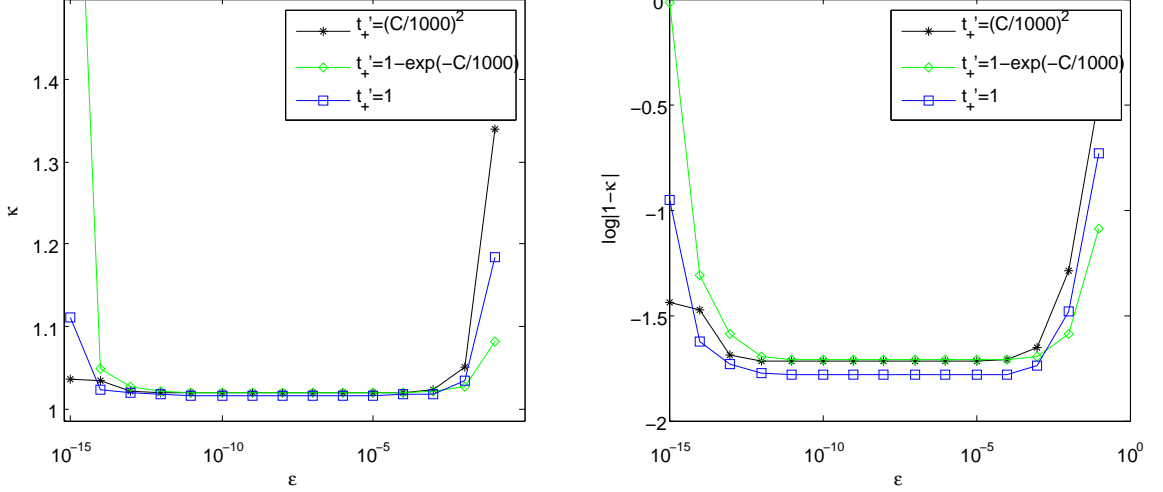
Figure 4.5: κ test to validate $\nabla_{t_+'}^{L_2} \mathcal{J}$ using three different perturbation function represented in linear and log scale

gradient $\mathbf{g}[\nabla \mathcal{J}]$ is given by,

$$
\begin{cases}
\mathbf{g}_0 \left[\nabla \mathcal{J} \right] = \nabla \mathcal{J}_0 \\
\mathbf{g}_n \left[\nabla \mathcal{J} \right] = \nabla \mathcal{J}_n + \frac{\nabla \mathcal{J}_n^T \nabla \mathcal{J}_n}{\nabla \mathcal{J}_{n-1}^T \nabla \mathcal{J}_{n-1}} \mathbf{g}_{n-1} \left[\nabla \mathcal{J} \right] \quad n = 1, 2, 3, ..,
\end{cases}
\tag{4.8}
$$

where n is iteration number. Along with the conjugate gradient, Brent line minimization technique is used to determine the optimal step length τ_n in each iteration. During the process of reconstruction visual examination of gradients and simulated fitting with experimental data is done to avoid undesirable characteristics in the reconstructed material properties. With consideration of all above mentioned components, the following algorithm is proposed for the reconstruction of material properties encompassing via the solution of the problem P1 and P2.

36

Algorithm 1 : Iterative minimization algorithm for finding material properties as a function of concentration.

Input: $\varepsilon_{\mathcal{J}}$ - adjustable tolerance, $l(n)$ - Sobolev parameter as function of iteration number, S - degree of smoothing, $\tilde{c}(x,t)$ - Experimental concentration values, $\tilde{D}$ $\tilde{t}_+$ - constant initial guesses for diffusion coefficient and transference number

Output: $D(c)$ and $t_+(c)$

Smooth the experimental data using Savitky-Goley filter with degree S

Solution of problem P1, $[\hat{t}_+ \ \hat{D}] \leftarrow \underset{t_+,D}{\operatorname{argmin}} \mathcal{J}$ using initial guesses $\tilde{D}$ and $\tilde{t}_+$

$D^{(0)} \leftarrow \texttt{ones}(\text{c}) \times \hat{D}$. Initial guess.

$t_+^{(0)} \leftarrow \texttt{ones}(\text{c}) \times \hat{t}_+$. Initial guess.

$n \leftarrow 1$

repeat

    solve governing equation and adjoint equation obtained by perturbing D.

    evaluate $\nabla_D^{L_2}\mathcal{J}$ and solve (3.33)-(3.34) to determine $\nabla_D^{H^1}\mathcal{J}$

    compute the conjugate direction $\mathbf{g}\left[\nabla_D^{H^1}\mathcal{J}\right]$ using (4.8)

    perform line minimization $\hat{\tau} \leftarrow \underset{\tau}{\operatorname{argmin}}\left\{\mathcal{J}\left(D^{(n-1)} - \tau\,\mathbf{g}\left[\nabla_D^{H^1}\mathcal{J}\right], t_+^{(n-1)}\right)\right\}$

    $D^{(n)} \leftarrow D^{(n-1)} - \hat{\tau}\,\mathbf{g}\left[\nabla_D^{H^1}\mathcal{J}\right]$

    solve governing equation and adjoint equation obtained by perturbing t_+.

    evaluate $\nabla_{t_+}^{L_2}\mathcal{J}$ and solve (3.33)-(3.34) to determine $\nabla_{t_+}^{H^1}\mathcal{J}$

    compute the conjugate direction $\mathbf{g}\left[\nabla_{t_+}^{H^1}\mathcal{J}\right]$ using (4.8)

    perform line minimization $\hat{\tau} \leftarrow \underset{\tau}{\operatorname{argmin}}\left\{\mathcal{J}\left(D^n, t_+^{(n-1)} - \tau\,\mathbf{g}\left[\nabla_{t_+}^{H^1}\mathcal{J}\right]\right)\right\}$

 $t_+^n \leftarrow t_+^{(n-1)} - \hat{\tau}\,\mathbf{g}\left[\nabla_{t_+}^{H^1}\mathcal{J}\right]$

    $n \leftarrow n+1$

until $|\mathcal{J}(D^{(n)}, t_+^{(n)}) - \mathcal{J}(D^{(n-1)}, t_+^{(n-1)})| < \varepsilon_{\mathcal{J}}|\mathcal{J}(D^{(n)}, t_+^{(n)}|$


To gain insight about the performance of the gradients and the convergence of the

algorithm, a toy problem is set up and the target concentration values are "manufactured" using an arbitrarily assumed diffusion coefficient function (resembling the actual dependence of D on c). The optimization to reconstruct diffusion coefficient is carried out with manufactured concentration values using L_2 gradients. In-situ experimental data that we have is available only in the sub domain of space and time, so to replicate this setup the manufactured concentration data only on a similar sub-domain is used for optimization. The range of simulated concentration in the sub domain is the Identifiability region. The result of optimization is presented in fig. 4.6a.

From fig. 4.6a the drawbacks of gradient in L_2 space is evident. The diffusion coefficient values D is very close to the target value in most of the identifiability region, but drops drastically to the initial guess close to the boundaries of identifiability regions. Some irregularities in the reconstructed diffusion coefficient can also be seen. Such drawbacks are avoided while using gradients in the H^1 space as shown in fig. 4.6b. Reconstruction of D(c) with H^1 gradients, as shown in fig. 4.6b, is also very close to the the profile of target D(c) and behaves much better near the boundaries of identifiability region than the reconstruction using L_2 gradient.
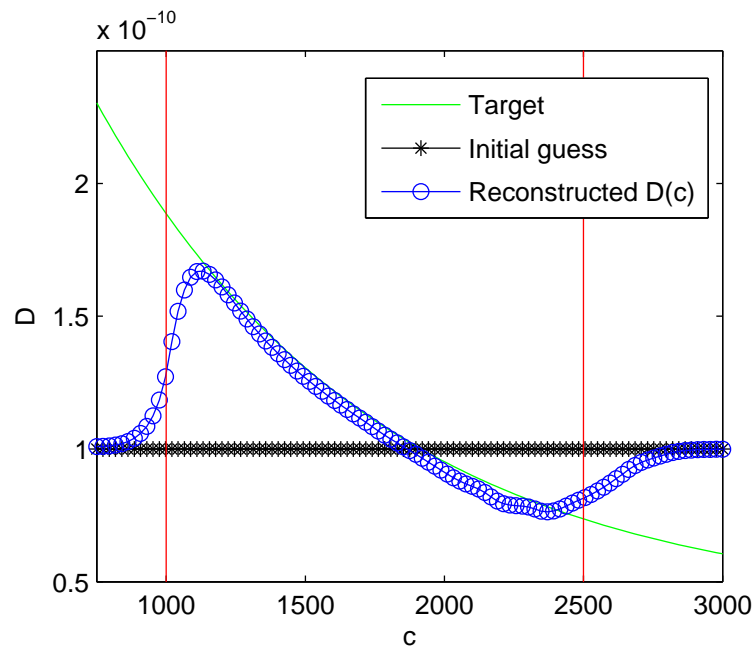
(a) Optimization using manufactured concentration values using $\nabla_D^{L_2}\mathcal{J}$. The vertical lines indicate the boundaries of identifiability region.
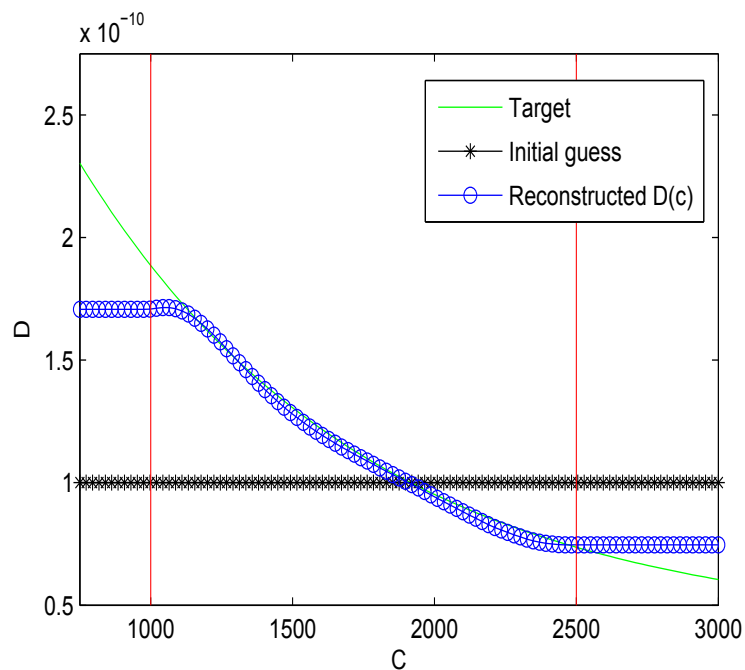
(b) Optimization using manufactured concentration values using $\nabla_D^{H^1}\mathcal{J}$. The vertical lines indicate the boundaries of identifiability region.

Figure 4.6: Algorithm validation using method of manufactured solution

Chapter 5

Results

5.1 Estimates of Constant Optimal $\widehat{D}$ and $\widehat{t}_+$

Here we show the results of solution of problem P1. Experimental data sets obtained using lab-prepared electrolyte is used for estimating material properties in Maxwell-Stefan's model and Fick's model and the result are shown in table 5.3. The initial guess in both models can be chosen arbitrarily as computational experiments shows that the optimization converges to the same minimizer for very wide range of initial guesses $D^{(1)}$ and $t_+^{(1)}$. The presence of uniqueness is also confirmed by the surface plots of the cost functional $\mathcal{J}(D, t_+)$ as a function of D and t_+, which is shown in fig. 5.1 and 5.2. The PDE solver, which is described in the section 4.2, is used to simulate the

	$D \times 10^{-10}$ $(m^2 s^{-1})$	t_+
Maxwell Stefan's	1.02	0.41
Fick's	0.98	0.41
Experiment	0.98	0.39

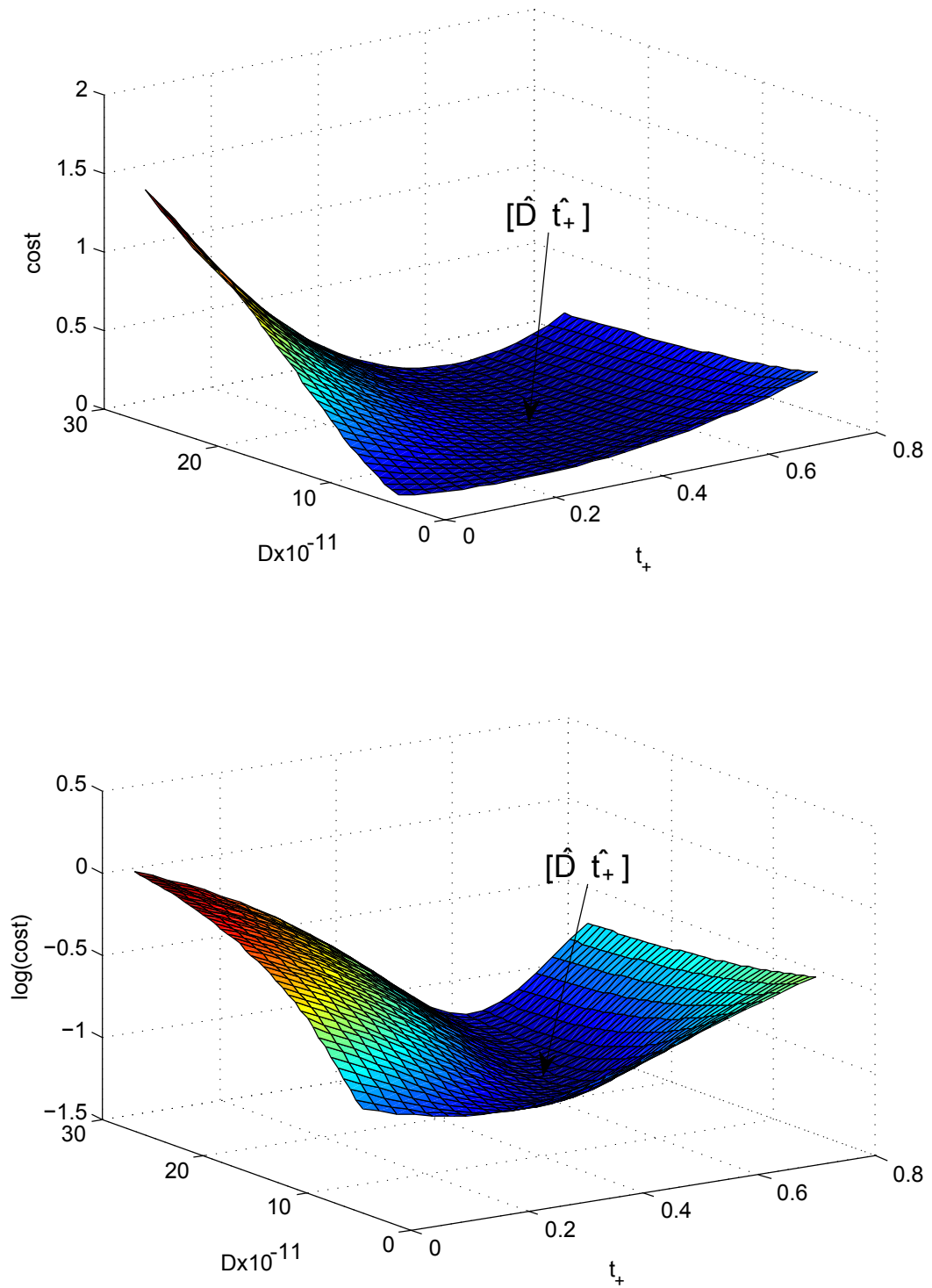Table 5.1: Optimization results and Experimental results for constant D and t_+

Figure 5.1: [Maxwell-Stefan's model] Dependence of cost functional $\mathcal{J}(D, t_+)$ on D and t_+ in linear and logarithmic scale.
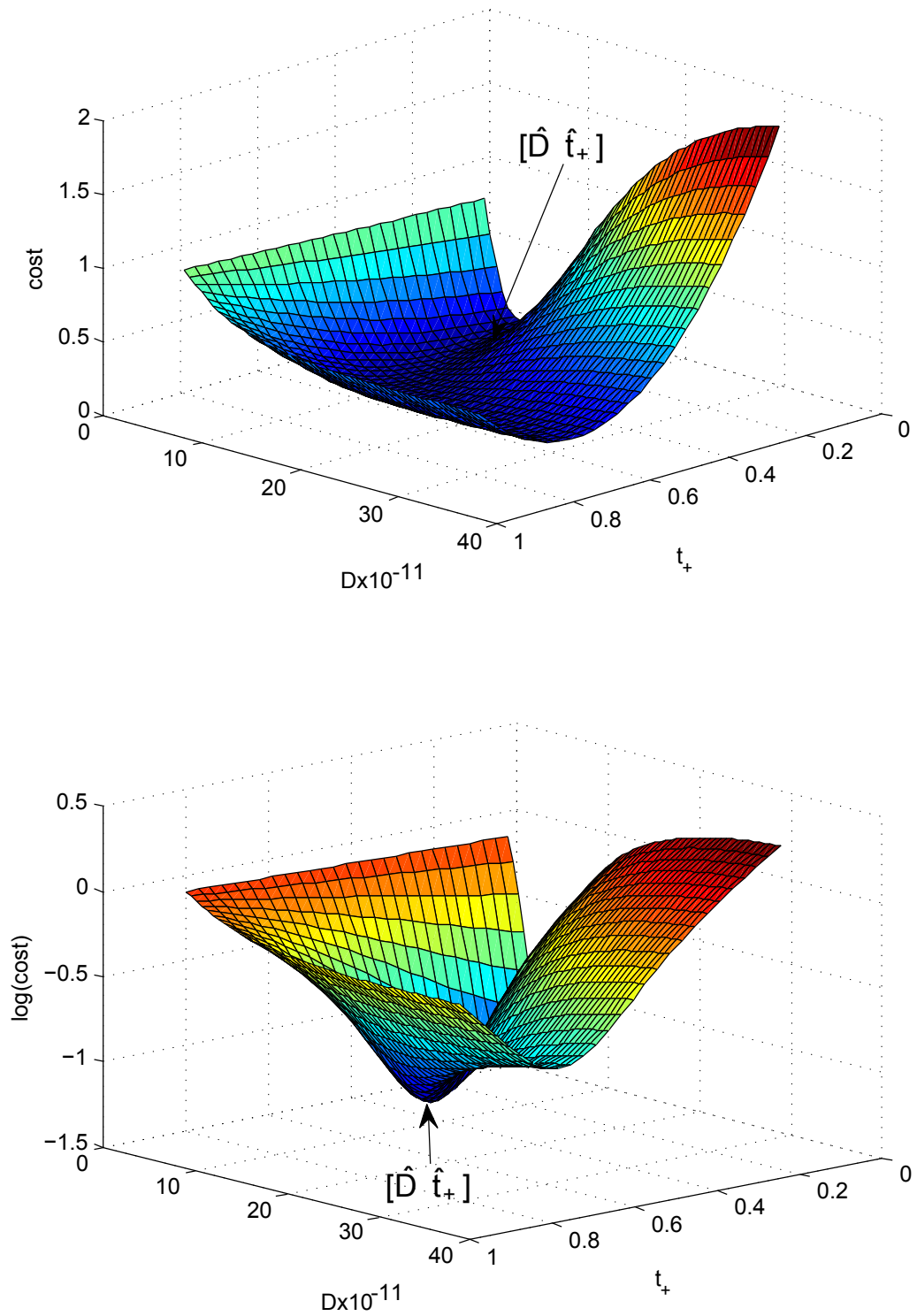
Figure 5.2: [Fick's model] Dependence of cost functional $\mathcal{J}(D, t_+)$ on D and t_+ in linear and logarithmic scale.

model (2.8) and (2.11) and the cost is calculated using eqn. (3.1). This calculated cost is passed to inbuilt MATLAB optimizer `fminsearch` with D and t_+ as the control variables. Tolerance for convergence was kept at 10^{-5} and the maximum number of iterations is fixed at 200. The constant diffusion coefficient $\widehat{D}$ and transference number $\widehat{t}_+$ obtained after optimization is compared against the experimental values measured using ex-situ NMR technique at $1000 mols/m^3$ concentration of electrolyte. We can see that that estimated parameters are in good agreement with experimental results. The simulated concentration values are shown together with the experimental data in fig. 5.3 and fig. 5.4 for Maxwell-Stefan's and Fick's model, respectively. It can be seen that the numerical simulation using estimated material properties fits well with the experimental concentration values.
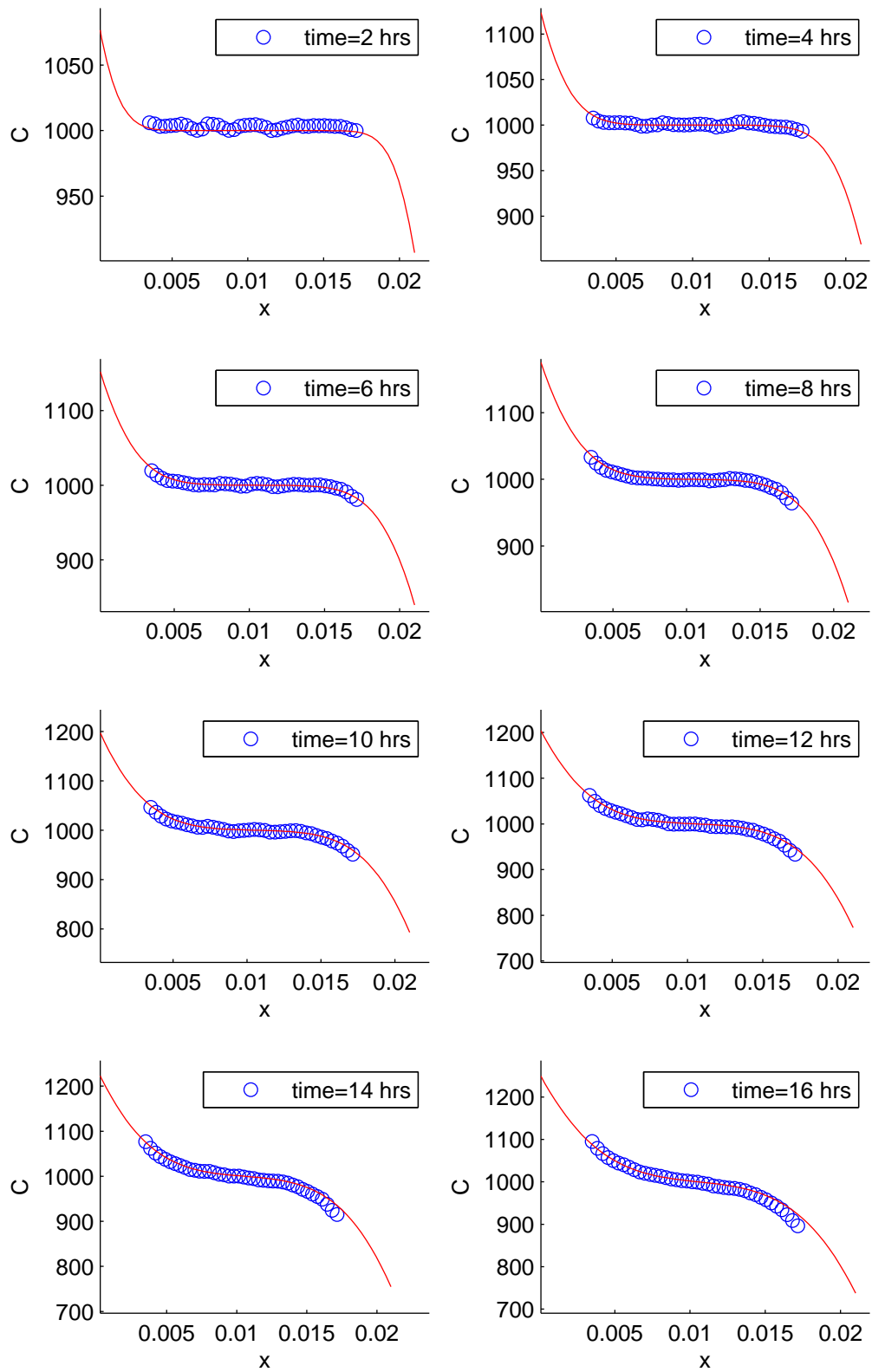
Figure 5.3: [Maxwell-Stefan's model] Experimental data (circles) and the concentration predicted by solving governing equations (2.8) (lines) with optimal $\hat{D}$ and $\hat{t}_+$ at different time levels
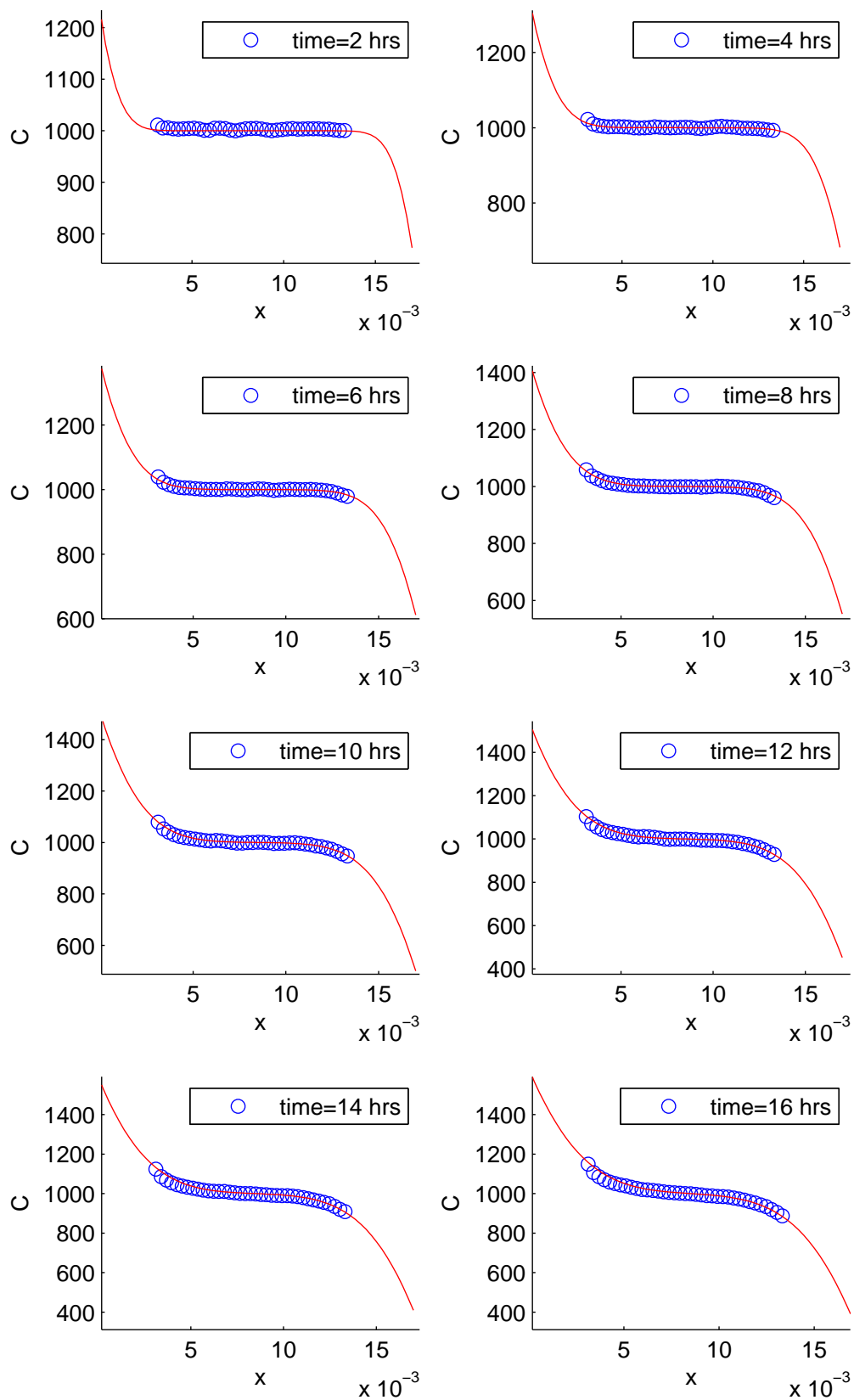
Figure 5.4: [Fick's model] Experimental data (circles) and the concentration predicted by solving governing equations (2.11) (lines) with optimal $\hat{D}$ and $\hat{t}_+$ at different time levels

45

5.2 Reconstruction of Concentration-Dependent $D(c)$ and $t_+(c)$

5.2.1 Maxwell-Stefan Model

Diffusion coefficient and transference number that appear in Maxwell-Stefan's model are reconstructed and the results are shown in fig. 5.5 and fig. 5.6, respectively. In this process we use Sobolev gradient (for conjugate gradient decent) obtained from L_2 gradients with Sobolev parameter l that varies from 1000 to 200 linearly with iteration for first 10 iterations and then fixed at value 200 for all iteration beyond the 10th. This enforces the low frequency features of the reconstruction to appear in the early stages of optimization and continuing to build the high frequency features through every subsequent iteration. It can be seen that diffusion coefficient decrease with increase in concentration as expected and the variation in diffusion coefficient value is about $0.4 \times 10^{-11} m^2 s^{-1}$ for the change in concentration value from $900 mol^1 m^{-3}$ to $1100 mol^1 m^{-3}$. In case of transference number, its value changes about 0.02 for the same change in concentration values.

Fig. 5.5 shows the reconstructed diffusion coefficient as the function of concentration in the identifiability region. The reconstructed D(c) value varies from value 1.01×10^{-11} to 1.42×10^{-11} in identifiability interval. Since we use homogeneous Neumann boundary condition while finding Sobolev gradient and the initial guess for D is constant, we see that the reconstruction predicts the function of D(c) with zero slope at the boundary of identifiability region and continues as constant outside it, which appears to be an artifact. This can be remedied by improving the quality of
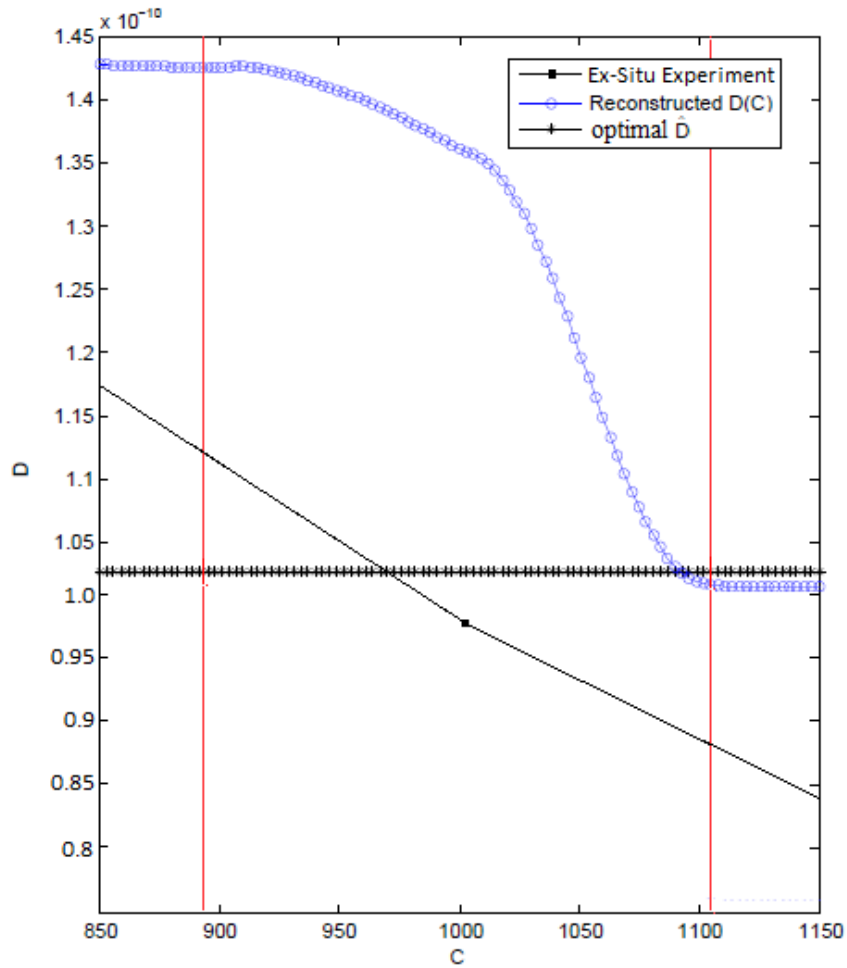
46

Figure 5.5: Reconstructed diffusion-coefficient of Maxwell-Stefan's model (2.8) compared against ex-situ experimental data. .Vertical lines denote the boundary of identifiability intervel.
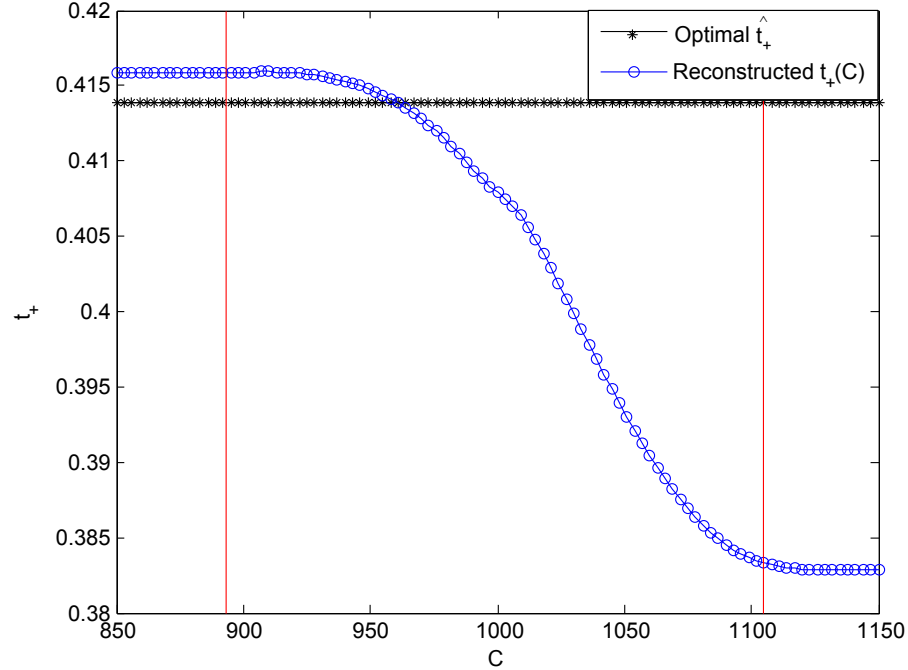
Figure 5.6: Reconstructed transference number of Maxwell-Stefan's model (2.8). .Vertical lines denote the boundary of identifiability intervel.

initial guess and the boundary condition of Sobolev gradient, which is a potential area of future exploration. Ex-situ experimental data for diffusion coefficient is also plotted in fig. 5.5. This diffusion coefficient is measured using the NMR self diffusion experiment with electrolytes prepared at different concentration of salt and diffusion coefficient is then constructed as a function of concentration by linearly interpolating all the data points. By comparing the reconstructed diffusion coefficient $D(c)$ with ex-situ experimental data, we can see that they don't match quite exactly but they fall under comparable ranges. This difference can be due to the fact that the ex-situ diffusion coefficient measures self diffusion coefficient that appears in Fick's diffusion model.

Transference number as a function of concentration is reconstructed and shown in

fig. 5.6. This reconstruction shows that $t_+(c)$ varies between 0.384 and 0.415 in the identifiability region. This variation is small but significant. Right now we are not able to identify any reliable experimental results to compare against the obtained $t_+(c)$ values with, but we can see that these results are consistent with various other studies which have probed the variation of transference number with concentration for common electrolytes such as solution of NaCl in water [17] and, on average in these studies, there is a 10% variation with decreasing trend of concentration in ranges similar to the identifiability region here, which is in good agreement with our result. While a quantitative comparison between these studies and our results is not possible due to different electrolytes used, the same qualitative trends are observed in both cases.

The reduction of cost functional during the reconstruction of D and t_+ is shown in fig. 5.7. It can be seen that between optimal constant and concentration-dependent material properties there is a very significant decrease in cost functional (from 0.089 to 0.010). From fig.5.8 we can also see that the simulated concentration profiles with reconstructed $D(c)$ and $t_+(c)$ matches with the experimental data much better than the simulated concentration profiles with optimal constant $\hat{D}$ and $\hat{t}_+$.

5.2.2   Fick's Model

The same approach of reconstruct diffusion coefficient and transference number that is explained in previous section is used here for Fick's model (2.11) and the results are shown in this section. Fig. 5.9 shows the reconstructed diffusion coefficient as a function of concentration. In this figure we can see that the reconstructed diffusion coefficient is in better agreement with the experimental data. The value of diffusion
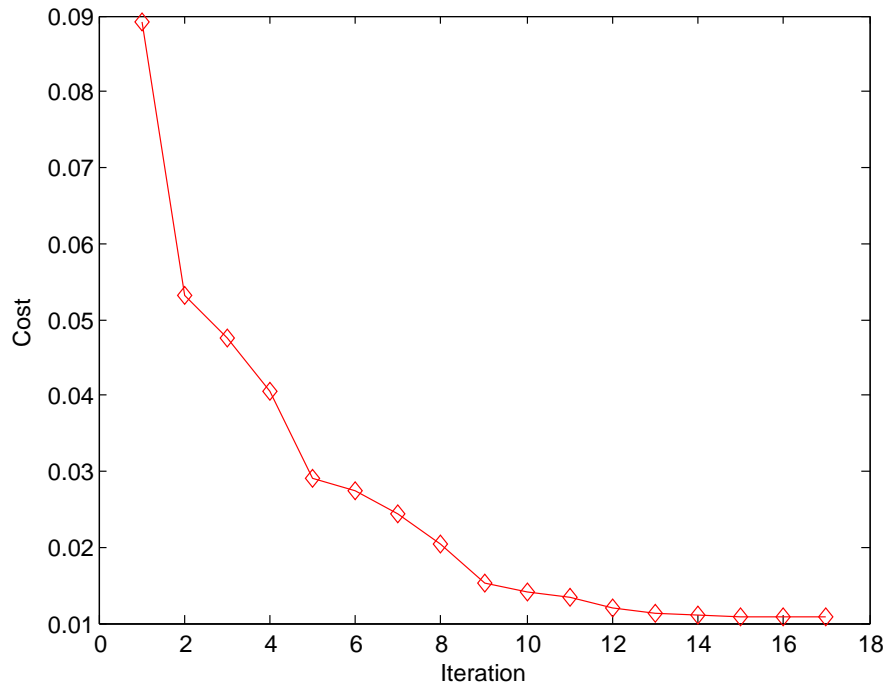
Figure 5.7: [Maxwell-Stefan's model] Cost decline during reconstruction
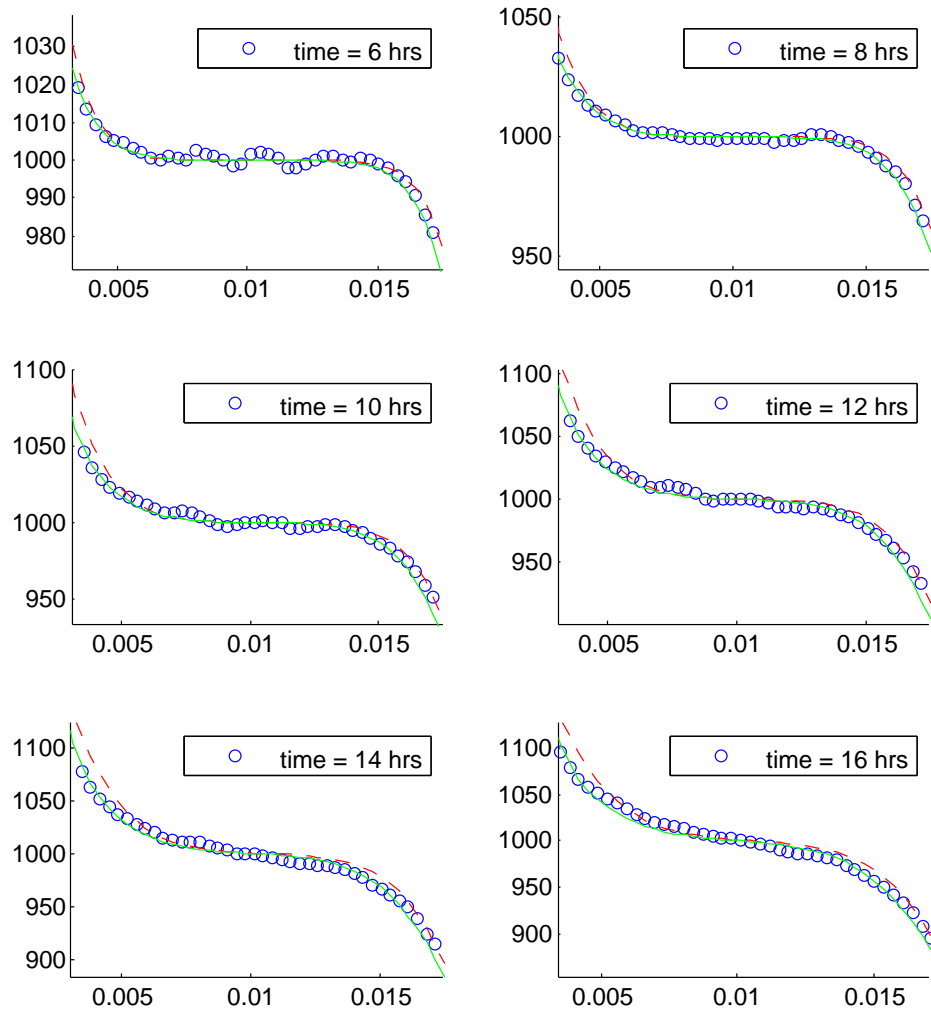
Figure 5.8: [Maxwell-Stefan's model] Comparison of experimental data with simulated data that are scaled up in X and Y axis to see the visible changes. Circles - experimental data, Dashed line - Simulated after constant D and t+ optimization, Solid line - Simulation after variable D and t+ optimization. space and concentration values are in X and Y axis respectively.
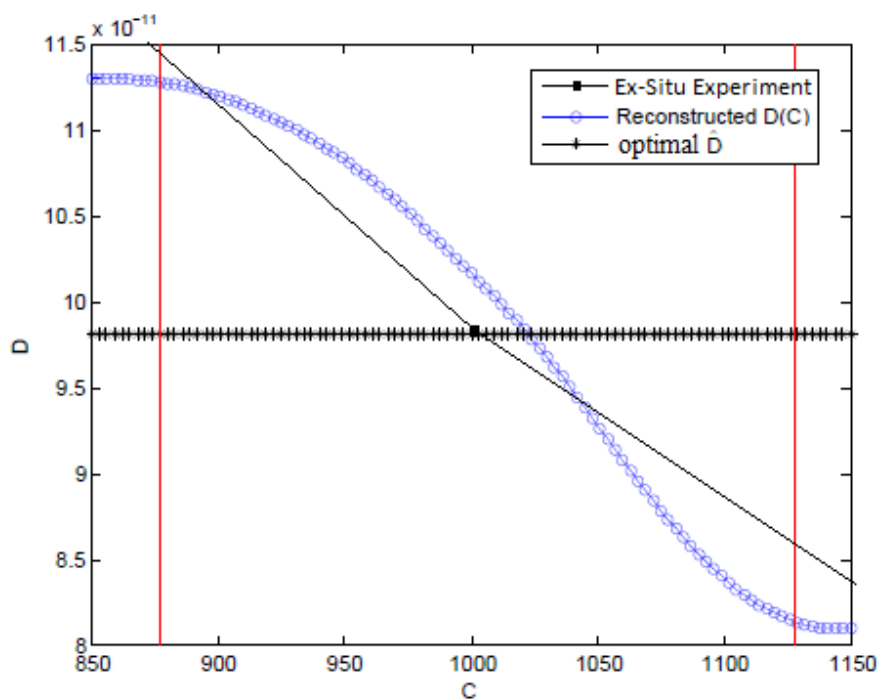
Figure 5.9: Reconstructed diffusion-coefficient of Fick's model (2.11) compared against ex-situ experimental data..Vertical lines denote the boundary of identifiability intervel.
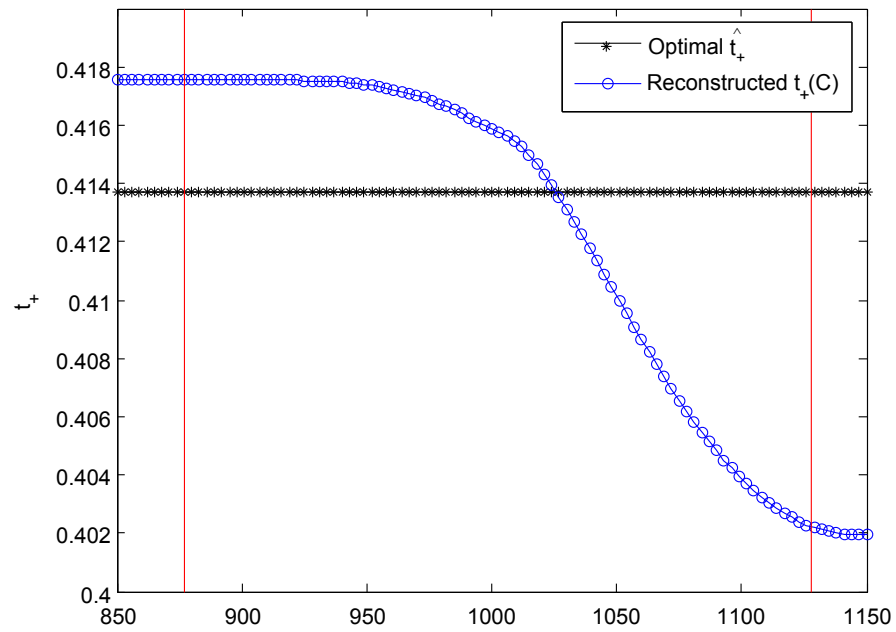
Figure 5.10: Reconstructed transference number using Fick's model (2.11).Vertical lines denote the boundary of identifiability intervel.
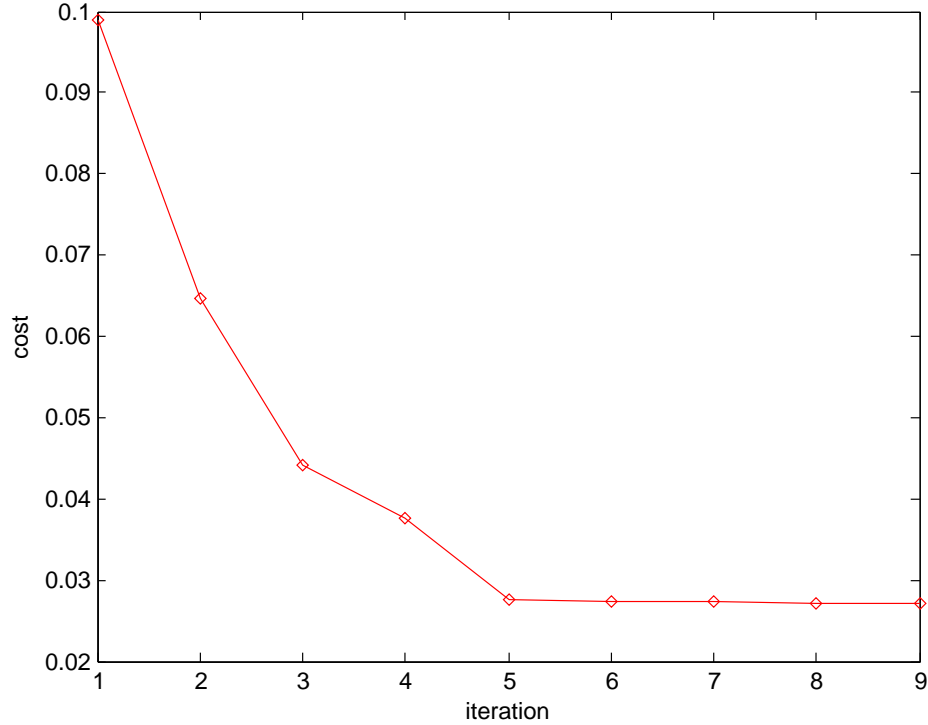
Figure 5.11: [Fick's model] Cost decline during reconstruction

coefficient varies between 8.1×10^{-11} to 11.2×10^{-11} on the identifiability interval and closely follows the ex-situ experimental diffusion coefficient values. Transference number on the other hand is similar to the result shown in previous section and varies between 0.4 and 0.42 and we do not have definitive experimental result to compare this value against, but as said in previous section this result is comparable with the experimental results obtained for other electrolytes as discussed in various other studies [17]. The cost value decreases from the value of 0.1 to 0.028 when we go from optimal constant $\hat{D}$ and $\hat{t}_+$ to reconstructed variable $D(c)$ and $t_+(c)$. This cost decline is significant and can be visually seen in fig. 5.12.
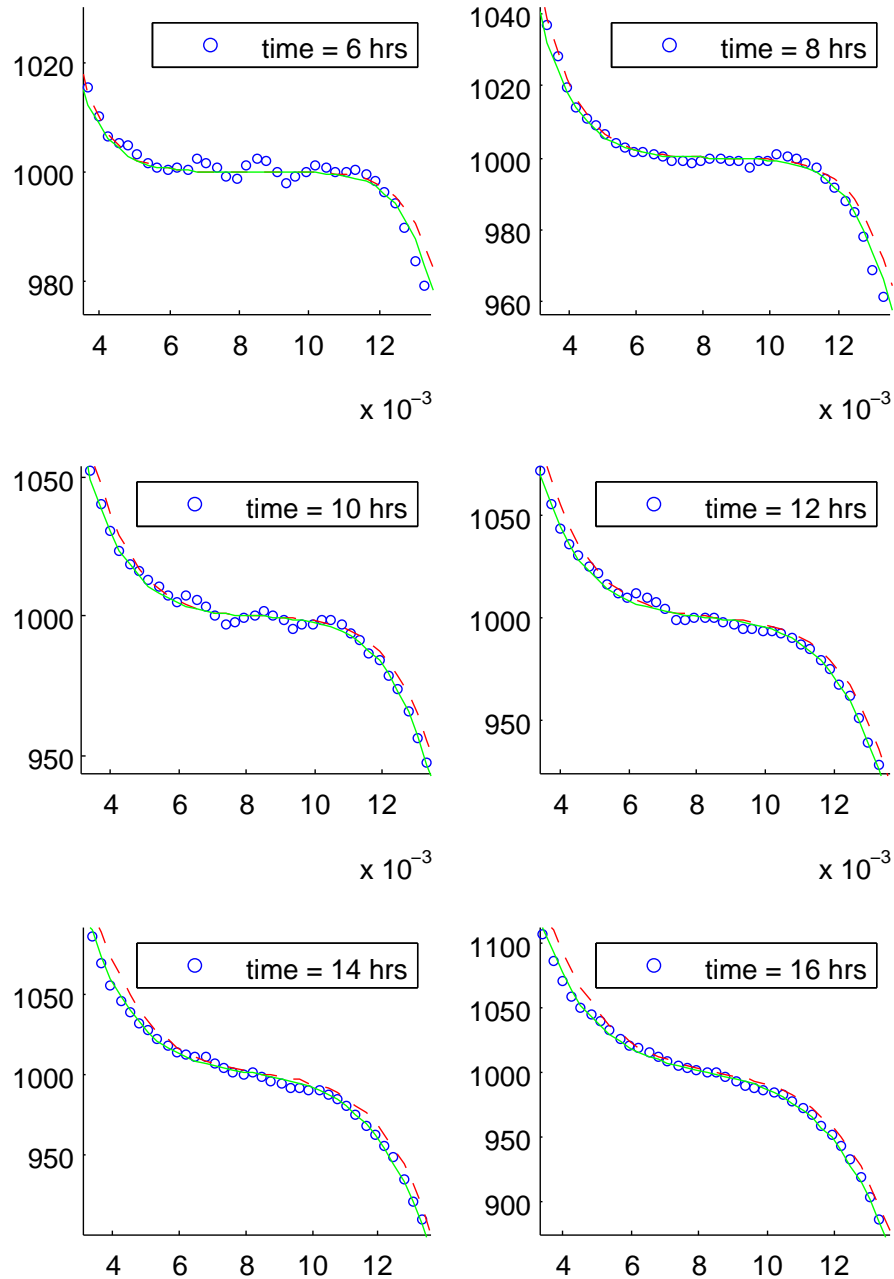
Figure 5.12: [Fick's model] Comparison of experimental data with simulated data that shows narrow ranges of c and t to see the visible changes. Circles - experimental data, Dashed line - Simulated after constant D and t+ optimization, Solid line - Simulation after variable D and t+ optimization. space and concentration values are in X and Y axis respectively.

5.3 Reconstruction for Standard Electrolyte using Fick's Model

Now that we have concluded from the previous section that Fick's model diffusion co-efficient matches well with the ex-situ experimental results, an attempt was made to reconstruct D(c) and $t_+(c)$ for the wider identifiability region. In this experiment, the quality of data was also substantially improved by our experimental colleagues and the data was less noisy than the data used in previous sections. In this experiment a constant current of $50\mu A$ is passed through the electrolyte and concentration data is collected as described in section 2.1. For this experiment a commercial electrolyte purchased from Novalyte Ltd. is used and Ex-situ diffusion values are obtained for the lab made electrolytes with same composition at different concentration of salt ($LiPF_6$ in EC/DMC).

	$D \times 10^{-10}$ $(m^2 s^{-1})$	t_+
Fickian-$\hat{D}$	2.91	-0.21
Experiment	2.33	0.39

Table 5.2: [Standard electrolyte-experiment 1] Optimization results and Experimental results for constant D and t_+

Results show that the transference number is in the range around -0.2, which by definition is not possible. To make sure that the obtained result is not a local minima, dependence of cost functional $\mathcal{J}(D, t_+)$ on D and t_+ as shown in fig. 5.13 is generated. It confirms that the obtained minima is in fact global. It was also
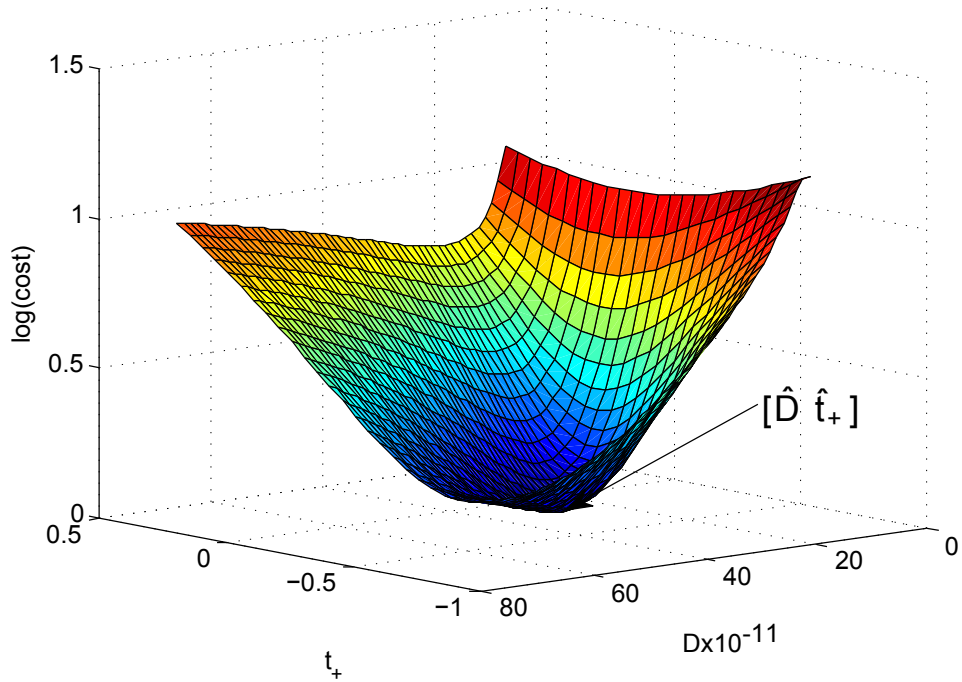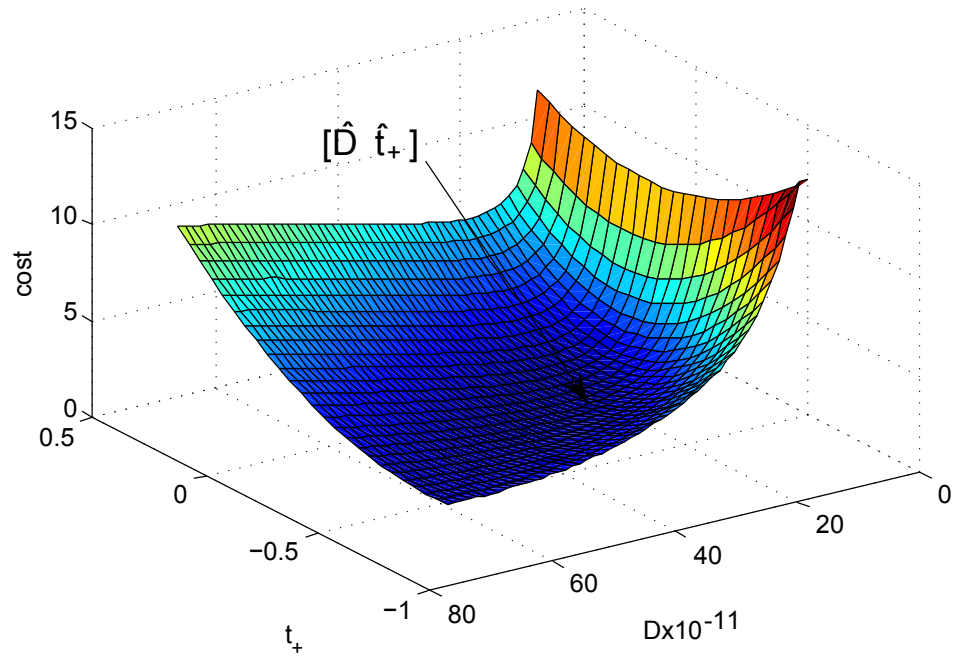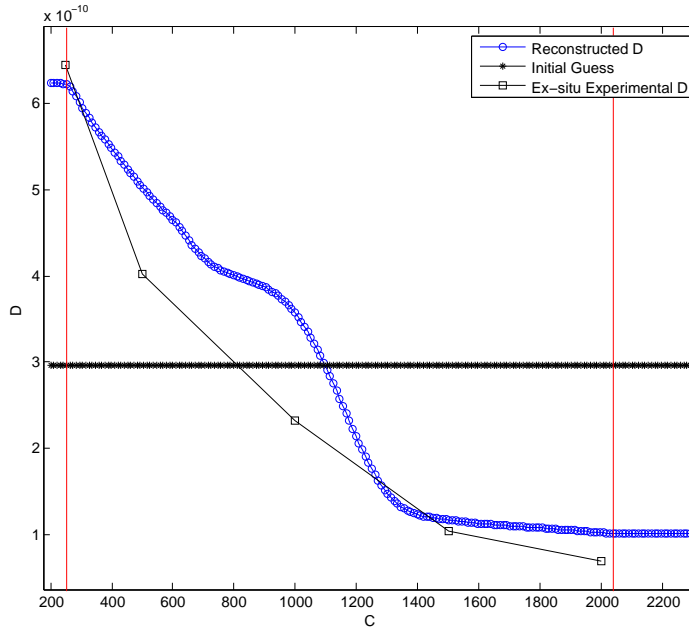
Figure 5.13: [Standard electrolyte-experiment 1] Dependence of cost functional $\mathcal{J}(D, t_+)$ on D and t_+ in linear and logarithmic scale.

(a) Reconstructed diffusion-coefficient of Fick's model (2.11) compared against ex-situ experimental data. Region between vertical lines denote identifiability interval.
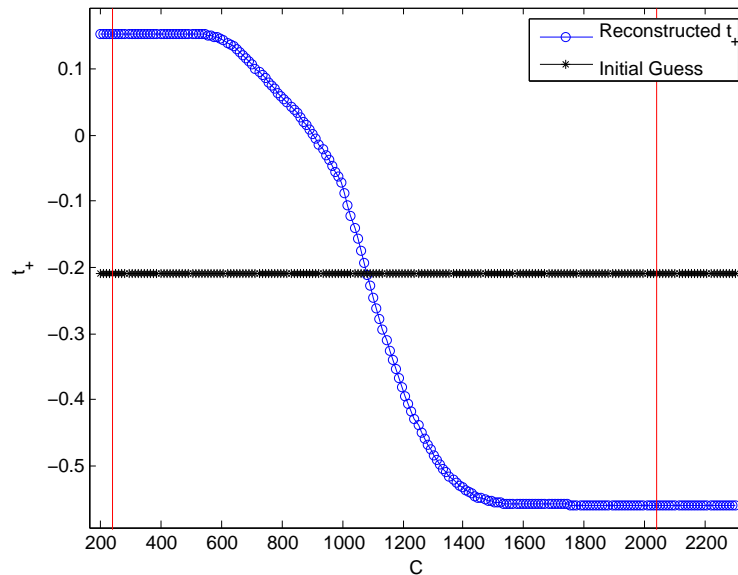
(b) Reconstructed transference number using Fick's model (2.11) . Region between vertical lines denote identifiability interval.

Figure 5.14: [Standard electrolyte-experiment 1] Reconstructed material properties.

speculated that this might be the effect of multiple local minima in the functional space of $D(c)$ and $t_+(c)$, so another algorithm was designed, by slight modification of original algorithm, which fixes t_+ as constant and reconstruct D as function of concentration. Using this algorithm, optimal cost value is obtained for wide range of transference number and results are plotted in fig. 5.15. This result indicates that the solution space might just have only global minima and reinforces our confidence in th results shown in the previous sections as well. Now, that multiple global minima factor is eliminated, it makes one think that there might be other phenomena that could have been unaccounted for. There are published documents that show negative transference number measurements [12] and there are various factors discussed in literature such as ion paring and clustering [25], precipitation [10, 12], phase change [10], density variation with concentration[13] etc., that may affect the concentration profile. During the experiment, we do not see any visual precipitation or phase change and the experiment was set up in such a way that the gravity has no effect. This leads us to think mainly about the ion coupling and ion clusters as reason for unrealistic results.

By analyzing the negative transference numbers, we can say that according to the current model (2.11), negative ions move in way that they use unrealistically large current (more than the supplied current). If ion coupling or ion clustering happens in the electrolyte, there will be neutralized anion-cation pair or ion cluster that will not move in the applied electric field and this will result in the stagnation of Lithium in the form of ion pair or ion cluster near cathode. This phenomenon will significantly increase the concentration of salt near the cathode and deplete the concentration near the anode. Therefore it may appear that negative ions using more current than the
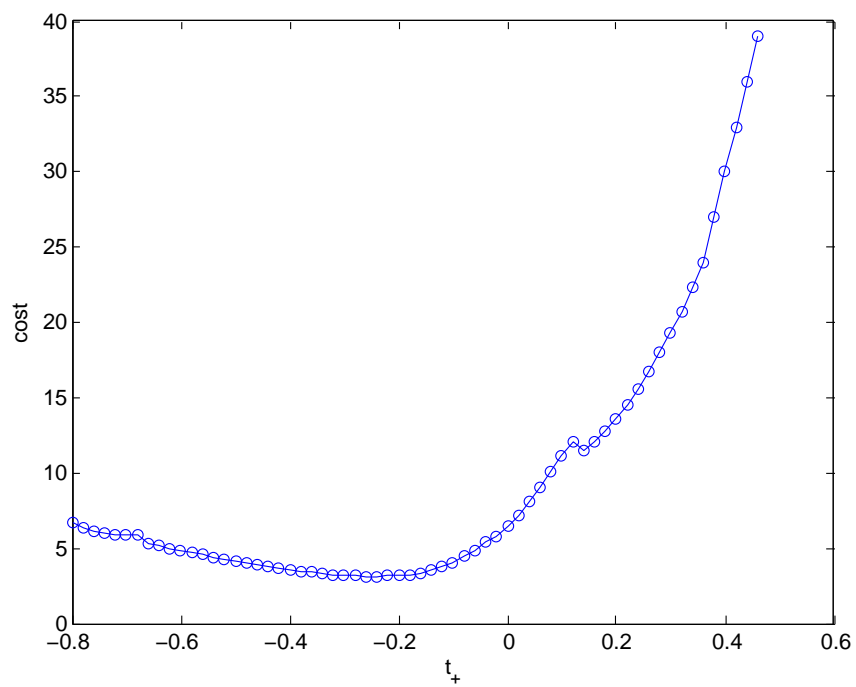
Figure 5.15: Transference number plotted against the cost obtained after reconstructing D(c) with constant t_+.

supplied current. This effect can be eliminated by applying low current and reducing the range of identifiability region.

Thus in the next experiment this is implemented by applying a lower current of $35\mu A$ and the results are shown in table 3 and fig. 5.16 - 5.17b.

	$D \times 10^{-10}$ $(m^2 s^{-1})$	t_+
Fickian-$\hat{D}$	3.9	0.18
Experiment	2.33	0.39

Table 5.3: [Standard electrolyte-experiment 2] Optimization results and Experimental results for constant D and t_+

In experiment 2 we can see that the transference number is positive but still in the lower range. Optimal constants $\hat{D}$ and $\hat{t}_+$ significantly deviate from the ex-situ NMR experiments. By reducing the current and identifiability range there is a significant change in transference number value from negative to positive, which suggests that there may be indeed the formation of ion pairs and clusters. To predict the mass transport in electrolyte with ion clustering and ion paring effect, we must include this phenomenon in the mass transport model equations (2.8) or (2.11), which is currently not within the scope of this thesis. However these results are shown to emphasize the fact that the developed tool can be very useful to validate the models used for material transport.
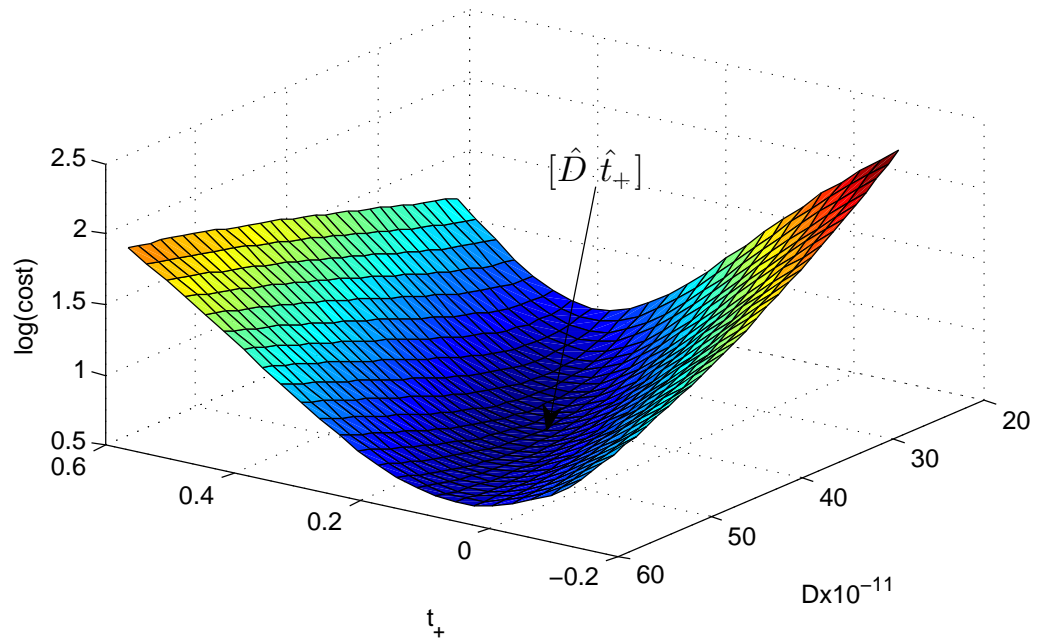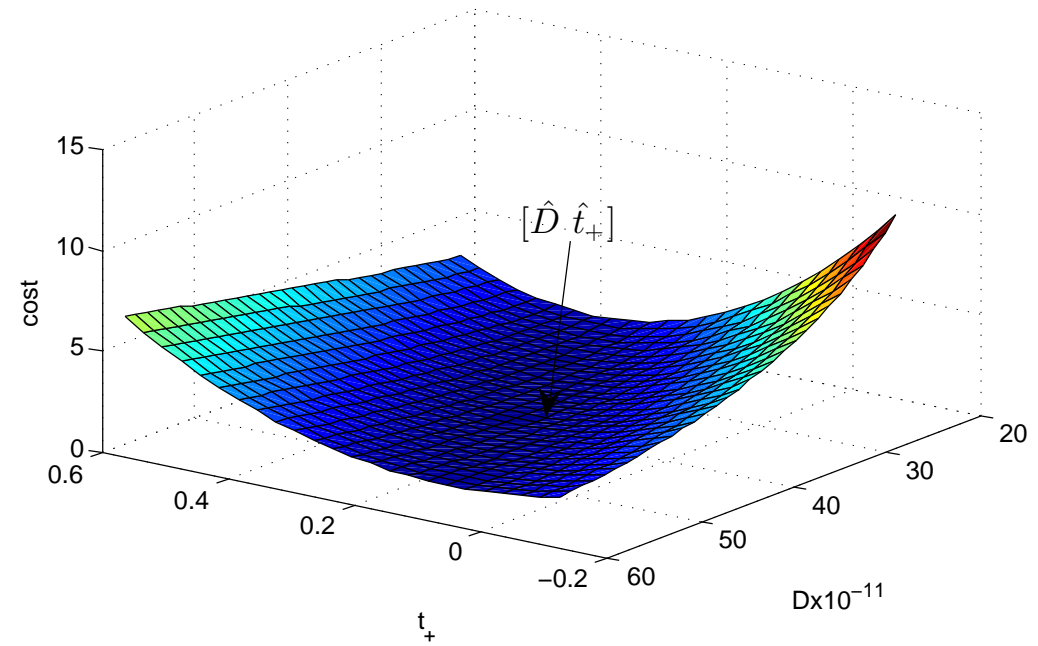
Figure 5.16: [Standard electrolyte-experiment 2] Dependence of cost functional $\mathcal{J}(D, t_+)$ on D and t_+ in linear and logarithmic scale.
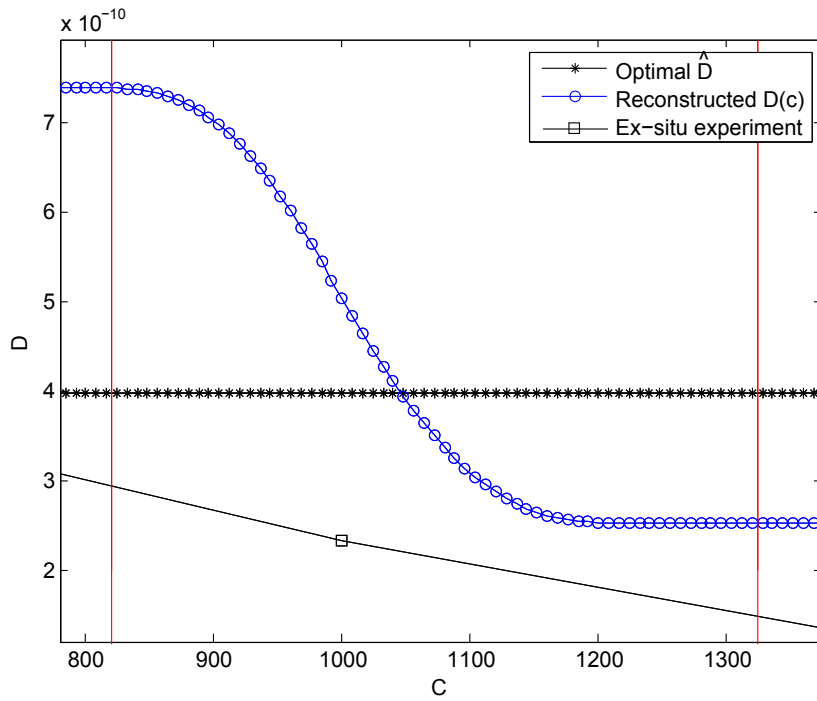
(a) Reconstructed diffusion-coefficient of Fick's model (2.11) compared against ex-situ experimental data. Region between vertical lines denote identifiability interval.
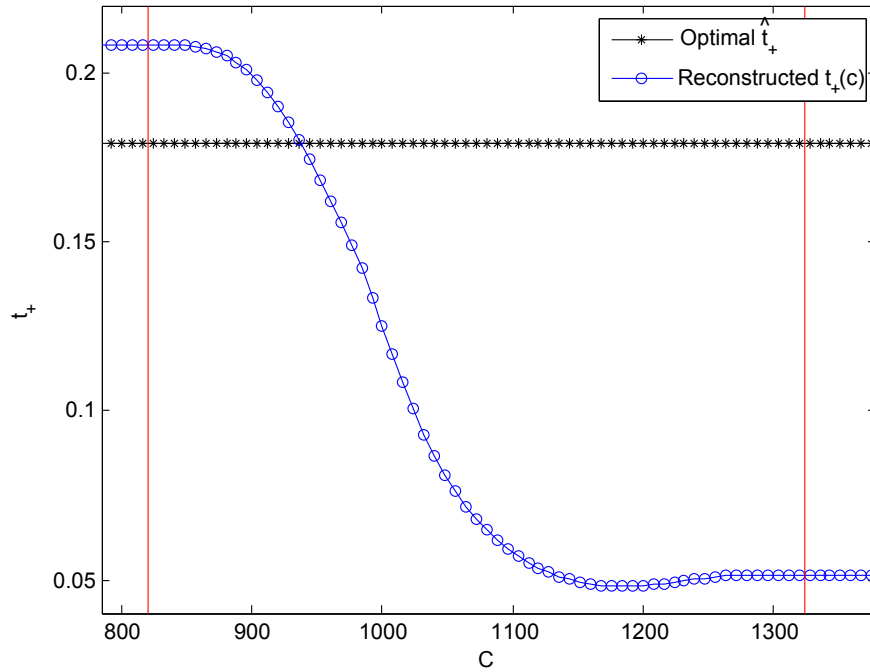
(b) Reconstructed transference number using Fick's model(2.11). Region between vertical lines denote identifiability interval.

Figure 5.17: [Standard electrolyte-experiment 2] Reconstructed material properties.

Chapter 6

Conclusion and Outlook

In this study, models for material transport in electrolyte were considered based on Maxwell-Stefan diffusion and Fick's diffusion and an algorithm was developed to obtain the material properties and their dependence on concentration. The algorithm was tested and validated at various levels, and then used to estimate the concentration-dependence of material properties of lab-made and commercial Li-ion battery electrolytes. From this study the following conclusions can be drawn.

- In contrast to various other research work [9, 22, 28, 13] that estimates material properties as constant using inverse problem, we can conclude from this study that we can estimate material properties that are dependent on the state using single experiment.

- Concentration profile obtained from in-situ experiment shows best match to the model that has concentration-dependent material properties and the cost functional was an order of magnitude smaller when compared with constant material properties. This emphasizes that the quality of Li-ion battery models

can be significantly improved by using material properties that are dependent on state.

- Diffusion coefficient in Fick's model is in good agreement with ex-situ NMR self-diffusion coefficient measurements and this demonstrates good reliability of this proposed method to estimate diffusion coefficient.

- Though the transference numbers (t_+) that are predicted as function of concentration have to be independently validated with a reliable method, it is shown that the t_+ values are in the expected range for smaller identifiability regions. However, for larger identifiability region the method predicts negative transference number and this prediction is wrong for obvious reasons. It is also shown that the solution space does not have multiple minimizing solutions and the reconstruction method used here cannot be the reason for the non-physical predictions. On the other hand, there is some evidence that the model that is used may not be correct and formation of ion pairs and clusters may play a significant role in material transport.

- we wish to emphasize the following facts.

    - The electrolyte used in section 5.3 is commercially used in Li-ion batteries.

    - The concentration ranges in standard electrolyte experiment 1 is very similar to the ranges seen in normal Li-ion battery operation.

    - The model used here is the one that is mostly used for physics based models of ion transport in electrolytes of Li-ion battery.

With these facts, this study records that the present ion transport models used

for modeling Li-ion batteries may not be sufficient to account for all the factors that affect concentration of ions in electrolyte.

With these conclusions this study leaves many open questions that are yet to be answered. It is important to note that the methodology used here can further be improved to get better results. The following points are identified as potential future avenues of research in the area of modeling material transport of Li-ion battery electrolyte and estimating its material properties.

- Improving the quality of initial guess the reconstruction algorithm, so that the material properties outside the identifiability region is no longer a constant.

- Developing a similar algorithm for reconstruction of material properties for different and/or simpler experimental data. For example boundary data are easier to obtain experimentally in potentiostatic and galvanostatic experiments than the state value inside the domain itself. Our preliminary experience suggests that it is possible to estimate material properties as a function of concentration using this kind of experimental data.

- Identifying the apparent shortcoming of the electrolyte transport model and estimating the transference number for a larger identifiability region.

- Exploring the application of this techniques to the other parameters like conductivity and other parts of batteries such as active material and particle binder.

- Exploring the the use of this technique to predict diffusion coefficient of Lithium atom in the solid parts of the battery electrode by using concentration data obtained from electron microscopy techniques or boundary data from galvanostatic and potentiostatic experiments.

Bibliography

[1] D. Aurbach. Review of selected electrodesolution interactions which determine the performance of Li and Li ion batteries. *Journal of Power Sources*, 89(2):206–218, 2000.

[2] A. Beck and M. Teboulle. Preliminary reference Earth modelA Fast Iterative Shrinkage-Thresholding Algorithm for Linear Inverse Problems. *SIAM Journal on Imaging Sciences*, 2(1):183–202, 2009.

[3] V. Bukshtynov, O. Volkov, and B. Protas. On optimal reconstruction of constitutive relations. *Physica D: Nonlinear Phenomena*, 240(16):1228–1244, 2011.

[4] M. Chen and G. A. Rincon-Mora. Accurate electrical battery model capable of predicting runtime and I-V performance. *IEEE Transactions on Energy Conservation*, 21(2):504–511, 2006.

[5] D. Deng, M. G. Kim, J. Y. Lee, and J. Cho. Green energy storage materials: Nanostructured TiO2 and Sn-based anodes for lithium-ion batteries. *Energy and Environmental Science*, 2.

[6] R. Domingo and P. Marqui. Review of Methods for Solving the EEG Inverse Problem. *International Journal of Bioelectromagnetism*, 1(1):75–86, 1999.

[7] M. Doyle, T. F. Fuller, and J. Newman. Modeling of Galvanostatic Charge and Discharge of the Lithium/Polymer/Insertion Cell. *The Journal of Electrochemical Society*, 140(6):1526–1533, 1993.

[8] A. M. Dziewonskia and D. L. Andersonb. Preliminary reference Earth model. *Physics of the Earth and Planetary Interiors*, 25(4):297–356, 1981.

[9] J. T. Edward. Molecular volumes and the Stokes-Einstein equation. *Journal of Chemical Education*, 47(4):261–268, 1970.

[10] V. Etacheri, R. Marom, R. Elazari, G. Salitra, and D. Aurbach. Challenges in the development of advanced Li-ion batteries: a review. *Energy and Environmental Science*, 4(1):3243–3262, 2011.

[11] M. Galiski, A. Lewandowski, and I. Stpniak. Ionic liquids as electrolytes. *Electrochimica Acta*, 51(26):5567–5580, 2006.

[12] H. Hafezi and J. Newman. Verification and Analysis of Transference Number Measurements by the Galvanostatic Polarization Method. *Journal of Electrochemical Society*, 147(8):3036–3042, 2000.

[13] M. Klett, M. Giesecke, A. Nyman, F. Hallberg, R. W. Lindstrm, G. Lindbergh, and I. Fur. Quantifying Mass Transport during Polarization in a Li Ion Battery Electrolyte by in Situ Li NMR Imaging. *Journal of American Chemical Society*, 134(36):14654–14657, 2012.

[14] G. Kraaijeveld and J. A. Wesselingh. Negative Maxwell-Stefan diffusion coefficients. *Industrial and Engineering Chemistry Research*, 32(4):738–742, 1993.

[15] S. A. Krachkovskiy, A. D. Pauric, I. C. Halalay, and G. R. Goward. Slice-Selective NMR Diffusion Measurements: A Robust and Reliable Tool for In Situ Characterization of Ion-Transport Properties in Lithium-Ion Battery Electrolytes. *The Journal of Physical Chemistry Letters*, 4(22):3940–3944, 2013.

[16] F. Lantelmea, H. Groulta, and N. Kumagaib. Study of the concentration-dependent diffusion in lithium batteries. *Electrochimica Acta*, 45(19):3171–3180, 2000.

[17] L. G. Longsworth. Transference numbers of aqueous solutions of Potassium Chloride, Sodium Chloride, Lithium Chloride and Hydrochloric Acid at 25° by moving boundary method. *Journal of Americal Chemical Society*, 54(7):2741–2758, 1932.

[18] A. K. Louis. Inverse Problems in Medicine. In *Proceedings of the Third German-Italian Symposium Applications of Mathematics in Industry and Technology*, pages 227–287, 1989.

[19] T. Nakamura and T. Chib. Determining the equation of state of the expanding Universe: inverse problem in cosmology. *Monthly Notices of the Royal Astronomical Society*, 306(3):696–700, 1999.

[20] A. Nyman, M. Behm, and G. Lindbergh. Electrochemical characterisation and modelling of the mass transport phenomena in $LiPF_6ECEMC$ electrolyte. *Electrochimica Acta*, 53(22):6356–6365, 2008.

[21] A. D. Pasquier, I. Plitz, S. Menocal, and G. Amatucci. A comparative study

of Li-ion battery, supercapacitor and nonaqueous asymmetric hybrid devices for automotive applications. *Journal of Power Sources*, 115(1):171–178, 2003.

[22] W. S. Price. Pulsed-field gradient nuclear magnetic resonance as a tool for studying translational diffusion: Part 1. Basic theory. *Concepts in Magnetic Resonance*, 9(5):229–336, 1997.

[23] B. Protas, T. R. Bewley, and G. Hagen. A computational framework for the regularization of adjoint analysis in multiscale PDE systems. *Journal of Computational Physics*, 195(1):49–89, 2004.

[24] V. R. Subramanian, V. Boovaragavan, and V. D. Diwakar. Toward Real-Time Simulation of Physics Based Lithium-Ion Battery Models. *Electrochemical and Solid-State Letters*, 10(11):225–260, 2007.

[25] K. Tasaki. Computational Study of Salt Association in Li-Ion Battery Electrolyte. *Journal of Electrochemical Society*, 149(4):418–425, 2002.

[26] L. O. Valena and J. N. Reimersa. Transport Properties of $LiPF_6$-Based Li-Ion Battery Electrolytes. *The Journal of Electrochemical Society*, 152(5):882–891, 2005.

[27] C.Y. Wang and V. Srinivasan. Computational battery dynamics (CBD)electrochemical/thermal coupled modeling and multi-scale modeling. *Journal of Power Sources*, 110(2):364–376, 2002.

[28] C. J. Wen, B. A. Boukamp, R. A. Huggins, and W. Weppner. Thermodynamic and Mass Transport Properties of LiAl. *Journal of The Electrochemical Society*, 126(12):2258–2266, 1979.